ANALYTICAL STUDY OF MICROWAVE SEA BRIGHTNESS TEMPERATURES: A COMPOSITE SURFACE MODEL

Richard J. Wagner, et al

TRW Systems Group

Prepared for:

Office of Naval Research

December 1972

17608-6010-RU-00

ANALYTICAL STUDY OF MICROWAVE SEA BRIGHTNESS TEMPERATURES: A COMPOSITE SURFACE MODEL

Final Report

by

R.J. Wagner and P.J. Lynch

December 1972

Geography Programs
Earth Sciences Division
OFFICE OF NAVAL RESEARCH
Department of the Navy
Arlington, Virginia 22217

Contract N00014-71-C-0240
Task Number NR 387-051/1-14-71 (414)

TRW SYSTEMS GROUP
Theoretical Physics Group
One Space Park
Redondo Beach, California 90278

17608-6010-RU-00

ANALYTICAL STUDY OF MICROWAVE SEA BRIGHTNESS TEMPERATURES: A COMPOSITE SURFACE MODEL

Final Report

by

R.J. Wagner and P.J. Lynch

December 1972

Geography Programs
Earth Sciences Division
OFFICE OF NAVAL RESEARCH
Department of the Navy
Arlington, Virginia 22217

Contract N00014-71-C-0240
Task Number NR 387-051/1-14-71 (414)

TRW SYSTEMS GROUP
Theoretical Physics Group
One Space Park
Redondo Beach, California 90278

Unclassified

Security Classification

DOCUMENT CONTROL DATA - R & D

(Security classification of title, body of abstract and indexing annotation must be entered when the overall report is classified)

1 ORIGINATING ACTIVITY (Corporate author)	2a. REPORT SECURITY CLASSIFICATION
Theoretical Physics Group TRW Systems Group Redondo Beach, CA 90278	Unclassified
	2b. GROUP

3 REPORT TITLE

Analytical Study of Microwave Sea Brightness Temperatures: A Composite Surface Model

4 DESCRIPTIVE NOTES (Type of report and inclusive dates)

Final Report;

5 AUTHOR(S) (First name, middle initial, last name)

Richard J. Wagner and Philip J. Lynch

6 REPORT DATE	7a. TOTAL NO OF PAGES	7b. NO OF REFS
December, 1972	83	18

8a. CONTRACT OR GRANT NO	9a. ORIGINATOR'S REPORT NUMBER(S)
N00014-71-C-0240	17608-6010-RU-00
b. PROJECT NO NR 387-051/1-14-71(414)	
c.	9b. OTHER REPORT NO(S) (Any other numbers that may be assigned this report)
d.	

10 DISTRIBUTION STATEMENT

This document has been approved for public release and sale; its distribution is unlimited.

11 SUPPLEMENTARY NOTES	12. SPONSORING MILITARY ACTIVITY
	Office of Naval Research Washington, D.C.

13 ABSTRACT

The second-order geometrical optics theory of rough surface emissivity and sea brightness temperatures is extended to lower microwave frequencies by the introduction of a composite surface model, in which the diffraction effects of surface structure smaller than a wavelength are explicitly included. Sea brightness temperatures are calculated for a range of microwave frequencies, both polarizations, all observation angles, and a variety of environmental parameters. The results are in good agreement with experiment.

Preceding page blank

DD FORM 1 NOV 65 1473

Unclassified

Security Classification

14. KEY WORDS	LINK A		LINK B		LINK C	
	ROLE	WT	ROLE	WT	ROLE	WT
Sea brightness temperature						
Microwave radiometry						
Emissivity of rough surfaces						
Scattering from rough surfaces						
Sea state measurement						
Electromagnetic scattering and emission						
Rough surface shadowing and multiple scatter						
Composite surface						

TABLE OF CONTENTS

LIST OF ILLUSTRATIONS

I. INTRODUCTION

This report is the final one of a series describing our investigation of the effects of surface roughness on emissivity and, in particular, of the results of our calculations of the microwave brightness temperatures of the sea. Prior to this study the only theory of rough surface emissivity was that of Stogryn[1] who used, in the Peake representation[2] for the emissivity, a single-scatter geometrical-optics approximation for the surface-scattered electromagnetic fields. To the resulting equation for the thermal energy emitted by the sea surface was added the microwave energy originating in the atmosphere and scattered (also in the single scatter approximation) by the sea surface. The total energy leaving the surface (described in terms of an "apparent" or "brightness" temperature) was evaluated by Stogryn for a variety of wind speeds and observation angles. Stogryn's calculations provided the first insight into the dependence of radiometric measurements on sea state, polarization, and observation angle. However, it is readily shown[3] that Stogryn's theory gives erroneous results for surfaces with appreciable roughness. Use of the simple single-scatter approximation in the theory has been shown to lead to a non-physical creation or loss of energy with the result that calculated emissivities and sea brightness temperatures may differ significantly from the correct values.

The source of the inconsistency in the Stogryn method was identified and a correct geometrical optics formulation was developed, first for a cylindrical roughness model of the sea surface[4] and subsequently for a general two-dimensional roughness model.[5] It was shown in this series of reports by the authors that: (1) the single scatter approximation is inadequate and it is essential to include both surface shadowing and (at least) double scatter by the

randomly rough surface; (2) the corrected theory, in marked contrast to the Stogryn theory, conserves energy to a high degree of approximation; (3) the geometrical optics theory, including shadowing and double scatter, provides rigorous upper and lower bounds to the effect of surface roughness on the emissivity and brightness temperature; (4) application of the theory to the sea showed that, for wavelengths such that geometrical optics is appropriate, the effect of changing sea state on radiometric measurements can be calculated to a satisfactorily high degree of accuracy. The model used accommodates changing water temperature and salinity, varying atmospheric conditions, any sea state, all observation angles, and both polarizations. An exhaustive series of computer calculations were carried out to establish the dependence of measured sea brightness temperature on all the possible variables.[6] The effects of foam and spray on total brightness temperature were excluded from the model because of the lack of reliable experimental or theoretical data. Approximate semi-empirical models for the effects of foam and spray can be readily incorporated, however, as was illustrated in the case of the earlier cylindrical roughness model.[7]

Comparison of the calculated sea brightness temperatures with experimental values[6] showed good agreement for wavelengths in the neighborhood of 1 cm, while for longer wavelengths discrepancies appeared. This is to be expected, for the strict validity of geometrical optic requires the surface to have negligible curvature over distances of the order of a wavelength; with increasing wavelength the surface will be increasingly structured over wavelength-sized dimensions and deviations from the purely geometrical optics predictions would result. The qualitative effect of surface height variations within a wavelength (which we will refer to as "small-scale structure") can be predicted.[7]

The effect on a radiation field of surface structure of a given size decreases with increasing wavelength; indeed, for sufficiently long wavelengths roughness effects on scattered or emitted radiation must disappear entirely. Thus, for longer wavelengths, an increasing fraction of the rough surface will radiate as though it were smooth and the total roughness effect must diminish (assuming there is no strong periodic component in the height spectrum which would produce resonance effects). This general diminution of the roughness dependence of the emissivity is enhanced by the fact that the roughness parameter for components of surface structure with scales larger than the radiation wavelength is the mean-square slope, and for the case of the sea surface the mean-square slope associated with such large scale components is known to decrease with increasing wavelength. This expected general decrease in sensitivity of the sea brightness temperature to roughness, with decreasing frequency, was borne out by the experiments of Hollinger[8,9] for frequencies between 1.4 and 19.4 gHz and wind speeds of up to 14 m/s.

There are some additional theoretical and experimental arguments which have been advanced regarding the dependence of the sea brightness temperature on sea state for longer microwave wavelengths. The possibility exists that the geometrical optics model will continue to apply, but with the roughness parameter — the rms slope of the total surface — being replaced by a smaller "effective" rms slope which is wavelength dependent. This possibility, as well as the form of the effective roughness parameter, was suggested by Lynch[10] who formulated a theory of rough surface scattering for wavelengths sufficiently long that significant surface curvature may exist within dimensions of the order of a wavelength He found that, except for near-grazing angles, the scattered intensity is still described by the geometrical optics theory but

with the actual rms surface slope replaced by a reduced rms slope whose value depended on both wavelength and observation angle; the same behavior would carry over to the emission problem. Similar conclusions were suggested by Hollinger[8] who showed that his data for the change in brightness temperature with wind speed, at a fixed observation angle, could be fit by the geometrical optics theory provided one assumed an effective rms slope for the surface whose value decreased with increasing wavelength.

However, to relate sea brightness temperatures to widely varying sea surface, atmospheric, and measurement conditions with sufficient accuracy to permit the use of a passive microwave system as a viable tool for remote measurement of sea surface conditions, a more precise theory or model of rough surface emissivity is required. The geometrical optics theory, developed in our earlier reports, is evidently adequate for frequencies of about 20 gHz and higher, but for lower frequencies a more general theory is needed. The required generalization, which includes the effects of both large and small-scale surface structure on sea brightness temperature, is described in this report. In Section II we discuss our general approach to the problem, the definition of the composite surface model, and the form of the wave height spectrum. In Section III the theory of the emissivity of an anisotropic, slightly rough random surface is applied to a modeling of the small-scale sea-surface structure and some numerical results are described. The equations used are a new representation for the emissivity, correct through second order in the roughness parameter, and are derived in the Appendix. Section IV contains a summary of the numerical results using the complete composite surface model of the sea. The model is shown to conserve energy at least as well as the geometrical optics model, and the relation between the upper and lower bounds to the sea brightness temperature —

developed originally in the context of the geometrical optics model — is shown to be preserved. The extensive numerical calculations of sea brightness temperature which were carried out for the composite surface model are summarized, with particular emphasis placed on the dependence on polarization, on frequencies in the range 1.4 to 20 gHz, on observation angle between 0° and 90° nadir angle, and on wind speeds from 0 to 20 m/s. In addition, comparisons are made with results based on the single-scatter geometrical optics theory of Stogryn, the shadow- and double-scatter corrected theory of Wagner and Lynch, and the experiments of Hollinger.

In this report we will lean heavily on concepts, equations, and results developed in our earlier reports and will refer to them freely without redefinition or repetition. For example, the definition of both the "Peake integral method," leading to the upper bound on the true brightness temperature, and the "direct emission method," leading to the lower bound, may be found in references 4 and 5; numerical results and conclusions based on both methods will be found in reference 6. In the present study, both methods were extended to include small scale structure but because of the greater accuracy of the direct emission method (a result established in ref. 6) all sea brightness temperature values quoted herein were calculated using this method. The geometrical optics equations also form the basic mathematical framework for the composite surface model. In this report we develop the modifications to these equations, but the equations themselves are quite lengthy and are not repeated here; they may be found in ref. 5.

II. COMPOSITE SURFACE MODEL

For radiation wavelengths in the centimeter region there will be roughness of the sea surface having scales larger than, comparable to, and smaller than the radiation wavelength. The effect on the emissivity of swells and large gravity waves can be satisfactorily treated by the geometrical optics theory while small gravity and capillary waves require a perturbation analysis, described in the next Section. Since only large and small scale roughnesses (relative to wavelength) are amenable to analysis, we assume the total roughness spectrum to be divided into two parts with each part treated by the appropriate method. The small waves ride on top of the large waves so that the mean plane of the random height variations over a small patch of emitting surface is not the horizontal ($z = 0$) plane but is the randomly oriented local tangent plane of the underlying large wave. The mean radiation emitted into a particular direction is therefore the superposition of the mean intensities emitted by arbitrarily oriented elements of surface area containing the small waves, weighted by the probabilities of occurrence of the possible oreintations (i.e., by the two-dimensional slope density of the large-scale structure). The addition of intensities emitted by contiguous elements is justified by the incoherence of thermal radiation (note however that in the scattering of thermal radiation some degree of interference is possible).

It is evident that the emission from the composite surface is described in precisely the same way as in the direct emission method[5] in the geometrical optics model, provided (1) the emissivity of an element of surface area is taken to be that of a patch of water containing small scale roughness instead of the emissivity of a patch of smooth water, and (2) the rms slope is that of

the large-scale structure alone rather than that of the entire surface. It was shown in an earlier report[6] that virtually all of the radiation reaching an observer arrives directly from the surface with at most a few percent reflected by the surface between the time of emission and observation. The small emission/reflection contribution to the emissivity will be calculated for the composite surface model as well. Since this second-order contribution is a small correction to the first order ("direct emission") term, we may make a convenient simplification in the calculation of the scattering by the small-scale structure of the radiation emitted by other portions of the surface. Because the wavelength is long compared to the roughness of the small component, the scattering by an element of surface will be sharply peaked in the local specular direction (i.e., relative to the mean plane of the surface element). Since the nonspecular component of the scattered radiation is quite small we may make the approximation that all the energy scattered by an element of surface area containing small-scale roughness appears in the local specular direction. In other words, we ascribe to the surface element an effective reflectivity r_s^i (i = the polarization index) defined by

$$r_s^i = 1 - \varepsilon_s^i \qquad (1)$$

where ε_s^i is the emissivity of the surface element and contains the contributions of the small scale structure (Sect. III).

Thus, once ε_s^i is known the emissivity of the total (composite) surface may be accurately calculated from the geometrical optics equations for the direct emission method, provided one makes the following transcriptions. If ε^i, r^i denote the emissivity and reflectivity of smooth sea water, then, wherever these quantities appear in the geometrical optics equations, one simply makes

the substitutions

$$\varepsilon^i \rightarrow \varepsilon_s^i$$

$$r^i \rightarrow r_s^i \quad . \tag{2}$$

In addition, the rms slope of the total surface is to be replaced by the rms slope of the large-scale wave structure as the pertinent roughness parameter. A slight revision in the equations is also required because the quantities ε_s^i, r_s^i now depend on the direction of the wind, relative to the directions of propagation and the local surface normal, whereas ε^i, r^i of course do not.

To the apparent emission temperature, calculated in this way, must be added the scattered sky radiation to obtain the total sea brightness temperature. The small scale surface structure will also affect the angular intensity distribution of the scattered atmospheric radiation. That is, although the radiation scattered by an element of surface area containing small-scale structure will be sharply peaked in the local specular direction, a small non-specular component will appear in other directions as well. It would be desirable to include the diffuse component in the single scatter term, although it could well be neglected in the smaller double-scatter contribution. This could in fact be done, although practical difficulties are encountered. The radiation leaving a given surface element, into a fixed direction, can originate from a large angular sector of the atmosphere because of the diffuse component of the scattering coefficients. Thus a solid angle integration over all source directions is required for every possible orientation of the surface element; averaging over all orientations then demands an additional double integration. Thus a 4-fold integration (not counting those required in the evaluation of the scattering coefficients themselves) must be performed

simply to calculate the single-scattered atmospheric radiation. Doing so would expand the present program beyond its intended scope, so a simplifying assumption will be made.

We assume, again, that all the energy scattered by the small structure on a surface element is concentrated in the specular peak with an intensity characterized by the modified reflection coefficient defined in Eq. (1). In this way, and with the use of Eq. (2), the approximate effect of the small-scale structure on both the single and double-scattered sky radiation may be calculated using the existing geometrical optics computer programs, provided only that ε_s^i is known and that the mean square slope of the large-scale structure is used as the geometrical optics roughness parameter. Some error is probably incurred as a result of this approximation. However, the longer wavelengths ($\gtrsim$ a few centimeters) are the region of our principal interest and, presumably, also the region of maximum effects of the small-scale structure; fortunately, it is also a region in which the intensity of the atmospheric microwave radiation is relatively low so that the error in the sea brightness temperature introduced by our approximation to the scattering coefficients is also diminished.

The most accurate method of calculating the apparent emission temperature, and therefore also the brightness temperature, was shown[6] for the geometrical optics case to be the "direct emission method" (which led to the lower bound on the true brightness temperature). This method will be even more precise for the composite surface model, for, as we have already shown, no approximations to the scattering coefficients are required to calculate the leading (direct emission) term, while the second-order (emission/reflection)

term is always sufficiently small so that our approximation to the diffuse scattering by the small-scale structure, required in this term, will introduce a negligible error in the emission temperature. In contrast, the "Peake integral method," which led to the upper bound on the true brightness temperature in the geometrical optics case, is intrinsically less accurate for several reasons. First of all, all terms in the expansion of the emissivity in terms of increasing orders of multiple scatter are larger than the corresponding terms in the same expansion of the direct emission representation; since third and higher orders of multiple scatter cannot be readily calculated, their neglect in both methods leads to a significantly larger error when the Peake representation is used than for the direct emission method. Secondly, the inclusion of small-scale structure is more difficult to do accurately, for the largest (single scatter) contribution requires explicit evaluation of the composite surface scattering coefficients; because of the magnitude of this term a simplified treatment of the diffuse scattering [as in, for example, Eqs. (1)-(2)] is not advisable and a much more complex analysis is required. This is also true of the second-order (double reflection) term which is an order of magnitude larger than the corresponding (emission/reflection) term in the direct emission representation. Finally, it must be noted that since the emissivity in the Peake method is derived from an integration over plane wave surface scattering coefficients, the possibility of coherent interaction of the fields scattered by the small structure lying on different surface elements of the large-scale structure must be considered; in the direct emission method this question does not arise.

For these reasons, the composite surface model based on the direct emission method is the one used for the calculation of the sea surface emissivity.

However, for purposes of comparison, it was also calculated using the Peake representation and the approximations of Eqs. (1) and (2), applied without further justification. The method was also used for a test of energy conservation, assuming a perfectly conducting surface.

We turn now to a consideration of the sea surface spectrum and a more precise definition of the "small" and "large"-scale surface roughness. If the height of the surface relative to its mean plane is given by a random function $z = \zeta(x,y)$, then the covariance function is the ensemble average

$$C(x,y) = \left\langle \zeta(x_o,y_o)\ \zeta(x_o + x,\ y_o + y) \right\rangle \tag{3}$$

and the vector wave height spectrum is its Fourier transform which may be written in the form

$$S(K_x,K_y) = \frac{2}{\pi^2}\int_{-\infty}^{\infty} dy \int_{0}^{\infty} dx\ C(x,y)\cos(K_x x + K_y y) \quad . \tag{4}$$

A polar representation in $\underline{K}$-space is convenient; with the transformations

$$\begin{aligned} K_x &= K\cos\Phi \\ K_y &= K\sin\Phi \\ S(K_x,K_y)\,dK_x dK_y &= S'(K,\Phi)\,K\,dK\,d\Phi \quad . \end{aligned} \tag{5}$$

A one-dimensional spectrum $S(K)$ and an angle-dependent factor $F(K,\Phi)$ may be defined as follows, assuming the x axis lies parallel to the wind direction,

$$\begin{aligned} KS'(K,\Phi) &= S(K,\Phi) \\ &= \begin{cases} S(K)F(K,\Phi), & |\Phi| < \pi/2 \\ 0 \quad\quad\ , & |\Phi| > \pi/2 \ . \end{cases} \end{aligned} \tag{6}$$

The anisotropy factor is assumed to be normalized such that

$$\int_{-\pi/2}^{\pi/2} F(K,\Phi)\,d\Phi = 1 \quad . \tag{7}$$

The composite surface is defined as follows. All harmonic components of the sea surface having wavelengths less than a few radiation wavelengths constitute the small-scale roughness, while all harmonic components with longer wavelengths are defined to be of large scale. Thus, if $k = 2\pi/\lambda$ is the radiation wavenumber and α a parameter to be specified, then the large-scale spectrum is

$$S_\ell(K) = \begin{cases} S(K) & , \quad K < \alpha k \\ 0 & , \quad K > \alpha k \end{cases} \tag{8}$$

and the small-scale spectrum is

$$S_s(K) = \begin{cases} 0 & , \quad K < \alpha k \\ S(K) & , \quad K > \alpha k \end{cases} \quad . \tag{9}$$

The union of the two is then the total spectrum

$$S(K) = S_\ell(K) + S_s(K) \quad . \tag{10}$$

Two derived quantities are required. One is the rms height, σ, of the small scale structure which is obtained from

$$\sigma^2 = \int_{\alpha k}^{\infty} S(K)\,dK \quad , \tag{11}$$

and the other is the rms slope in the x and y directions Σ_x, Σ_y of the large scale structure, given by

$$\Sigma_x^2 = \int_0^{\alpha k} dK\ K^2 S_\ell(K) \int_{-\pi/2}^{\pi/2} \cos^2\Phi F(K,\Phi)\ d\Phi$$

$$\Sigma_y^2 = \int_0^{\alpha k} dK\ K^2 S_\ell(K) \int_{-\pi/2}^{\pi/2} \sin^2\Phi F(K,\Phi) d\Phi \quad . \tag{12}$$

We note that for optical frequencies ($k \to \infty$) Eqs. (12) become the mean square slopes of the entire surface and their values should agree, at a given wind speed, with the experimental values of the upwind and crosswind slopes given by Cox and Munk.[11,12]

The equilibrium spectrum is fairly well known for low wavenumbers but for larger wavenumbers, particularly in the short capillary wave region, there is still considerable uncertainty in both the wave number and wind speed dependence. Choice of a suitable spectrum therefore involves some measure of arbitrariness. One form of the vector spectrum, continuous for all wave numbers, was suggested by Pierson.[13] We found, however, that the evaluation of Eq. (12) for optical frequencies gave slope values which were not in satisfactory agreement with the Cox and Munk results. A different form for the one-dimensional spectrum, S(K), was recently suggested by Wu,[14] who reanalyzed the Cox and Munk data in terms of a logarithmic dependence of mean-square slope on wind speed, and established new spectral constants for a Phillips-type spectrum. The Wu spectrum has wind-speed dependent cutoffs at both low and high wave numbers, plus a discontinuity at the start of the capillary range ($K_c \sim 360 m^{-1}$). One of the three discontinuities was removed by adjoining to the low end of the Wu spectrum the form suggested by Pierson.[13] In addition, the directionality factor $F(K,\phi)$ of Pierson was used to form the two-dimensional spectrum $S(\underline{K})$, which is then

$$S(\underline{K}) = \begin{cases} \dfrac{S_1(K)}{\pi K}\left[0.08\cos^2\phi + 2.56\cos^4\phi + (0.5 + 0.92\cos^2\phi - 2.56\cos^4\phi)\exp\left(-\frac{1}{2}g^2/K^2W^4\right)\right], & 0 < K < K_c \\ \dfrac{S_2(K)}{\pi K}\left(\frac{1}{2} + \cos^2\phi\right), & K_c < K < K_\nu \\ 0, & K_\nu < K \end{cases} \tag{13}$$

where $g = 9.8\ \text{msec}^{-2}$, W is the wind speed in meters per second, $K_\nu = 1.67\times10^{-2}K_cW^2$, and

$$S_1(K) = 4.6\times10^{-3}K^{-3}\exp(-.74g^2/W^4K^2)$$
$$S_2(K) = 3.15\times10^{-2}K^{-3} \quad . \tag{14}$$

These equations, together with Eqs. (8) and (9) define the "small-scale" and "large-scale" components of the sea surface.

The parameter α may be retained as an adjustable parameter to secure a best fit to the brightness temperature data. We chose instead to impose an additional constraint to fix α and then retain this value for all the calculations. The argument used to establish this constraint is as follows. The emissivity of a slightly rough surface can be evaluated through second order in the perturbation parameter $(k\sigma)$. To the extent that $k\sigma$ is sufficiently small that higher order contributions are negligible, this result will be exact. We therefore choose to include as much of the surface roughness as possible in the small-scale spectrum (i.e., α is to be as small as possible) while at the same time satisfying the requirement that $(k\sigma)^2 \ll 1$. Evaluation of Eq. (11) for a range of values of α led to the choice $\alpha = 0.2$. For this α we found

$(K\sigma)^2 \sim 0.06$, a value which remained nearly constant [because of the predominantly K^{-3} dependence of $S(K)$] over the range of frequencies and wind velocities of interest to us.

III. EMISSIVITY OF THE SMALL-SCALE ROUGHNESS

The solution of Maxwell's equations for the problem of a plane wave incident on a randomly rough interface between two media was obtained by Rice[15] by a perturbation method, for the case in which the wavelength is long compared to the rms excursions of the interface from its mean (planar) value. An harmonic representation was assumed for the components of the electric and magnetic fields and for the random boundary surface. Application of the differential equations and the boundary conditions then led to algebraic equations for the Fourier transforms of the fields on the boundary surface which could be solved for each order of perturbation. Explicit first-order solutions, for both horizontal and vertical polarizations of the incident field, and the second-order solution for horizontal polarization were given by Rice; the second-order vertical polarization result was later given by Valenzuela.[16] The spatial fields can be reconstructed from the Fourier coefficients and the mean intensity of the scattered radiation evaluated in terms of integrals over the surface height spectrum. A half-space integration over all scattering angles, for a fixed incident wave vector, then gives the mean total energy scattered by the surface: applying a statement of energy balance then yields the mean surface emissivity.

Such a procedure for calculating the emissivity is exceedingly cumbersome. However, the calculation may be considerably simplified. It is shown in the Appendix that the mean polarized emissivity, ε_s^i, may be expressed directly in terms of the Fourier coefficients of the scattered field and the

surface height spectrum. The equations derived there are for the case in which the z axis is normal to the mean plane of the surface and the observation direction lies in the x-z plane; the horizontal and vertical polarization components of the emissivity have the usual definition relative to this choice of coordinate axes.

It is necessary to transform the expressions for the emissivity components to an arbitrary orientation of coordinate axes, for the "mean plane" of the small-scale structure is to be an (arbitrarily oriented) element of surface area of the large-scale structure. A coordinate system has already been defined by the geometrical optics equations:[5] the $\underline{z}$ direction is normal to the mean plane of the entire sea surface, while the $\underline{x}$ direction was assumed to be parallel to one of the principal axes of the slope distribution, that is, parallel to the wind velocity vector $\underline{W}$. Now a local x', y', z' coordinate system on a surface element is defined such that $\hat{z}'$ is the direction of the normal, $\hat{n}$, to the element and $\hat{y}'$ is normal to the plane defined by $\hat{z}'$ and the wave vector $\hat{k}$ pointing toward the observer:

$$\begin{aligned} \hat{z}' &= \hat{n} \\ \hat{y}' &= \hat{z}' \times \hat{k}/|\hat{z}' \times \hat{k}| \\ \hat{x}' &= \hat{y}' \times \hat{z}' \quad . \end{aligned} \tag{15}$$

Now, the wind velocity at the surface is presumably parallel to the plane of the surface element, therefore we take the direction of the wind velocity vector $\hat{W}'$, in the local coordinate system, to be

$$\hat{W}' = (\hat{z}' \times \hat{W}) \times \hat{z}'/|\hat{z}' \times \hat{W}| \quad . \tag{16}$$

The angle ψ between the local wind vector and the local x direction is given by

$$\cos\psi = \hat{W}' \cdot \hat{x}' \quad . \tag{17}$$

Since $\psi \neq 0$, in general, the directional wave spectrum of the small structure, given by $S(K,\phi)$ in Eqs. (13), transforms on the surface element to

$$S_\psi(K,\phi) = S(K,\phi-x) \quad . \tag{18}$$

If s_x, s_y are the slopes of the surface element in the x and y directions, k_x the x-component of $\hat{k}$, and Θ the angle between $\hat{k}$ and the local surface normal, then it may be shown from the preceding equations that the random variable ψ is given explicitly by

$$\cos\psi = \left[k_x + \frac{s_x \cos\Theta}{\sqrt{1+s_x^2+s_y^2}}\right] \frac{\sqrt{1+s_x^2+s_y^2}}{\sqrt{1+x_y^2}\,\sin\Theta} \quad . \tag{19}$$

Since the emissivity equations in the Appendix refer to a local coordinate system, the spectrum (denoted by $W(\underline{K})$ in the Appendix) must be taken to be S_ψ, given by Eq. (18),

Finally, the "horizontal" and "vertical" polarization components of the emissivity also refer to the local coordinate system. The transformation to the fixed xyz coordinate system of the observer is also required and is given by

$$\begin{aligned} \varepsilon^h &= a_1^2\, \varepsilon'^v + b_1^2\, \varepsilon'^h \\ \varepsilon^v &= b_1^2\, \varepsilon'^v + a_1^2\, \varepsilon'^h \quad , \end{aligned} \tag{20}$$

where a_1 and b_1 were derived in an earlier report [Eqs.(5.13)-(5.16) of ref. 5].

This completes the specification of the equations required for the computation of the emissivity and brightness temperature of the sea surface in the composite surface model. Results of the computations are discussed in the next Section.

Before leaving the topic of the small-scale emissivity, we shall describe some of the numerical results for the case of a surface having only small roughness. In this case the mean plane of the surface is $z = 0$, the local and observer's coordinate systems coincide, and the emissivity equations of the Appendix apply without transformation. The emitting medium is assumed to be sea water and the spectrum to be the small-scale spectrum defined earlier, with a low-frequency cut-off of $0.2k$. The equations were evaluated numerically for observation angles of 0-90° measured from nadir, azimuthal angles of 0-90° relative to the wind direction, wind speeds of up to 30 m/s, a selection of frequencies between 1.4 and 100 gHz, and both polarizations. The parameter α was fixed, as described earlier, at a value of 0.2. The perturbation parameter ($k\sigma$) was relatively constant over most of the range of the parameters although at the higher frequencies and for large wind speeds it increased in value to a point where the validity of second-order perturbation theory may be questionable (e.g., at 100 gHz, $W = 14$ m/s, $k\sigma \sim 0.6$).

Since the flat surface emissivity of sea water is well known we show only the roughness effect, $\Delta\varepsilon \equiv \varepsilon$ (rough) $- \varepsilon$ (flat), in the accompanying figures. Figure 1 shows the dependence of $\Delta\varepsilon$ on observation angle for H polarization, $\nu = 1.4$ gHz, $\psi = 0°$ (upwind observation), and winds of 3, 4, 8 and 14 m/s. The maximum roughness effect shown would correspond to a change in effective emission temperature of about 2°K. Figure 2 shows the same cases but for cross-wind observation, $\psi = 90°$; a somewhat greater roughness effect is indicated. It was established that for all frequencies, polarizations, wind speeds, and observation angles the dependence on fetch angle ψ is given by

$$\Delta\varepsilon(\psi) = \Delta\varepsilon(0)\cos^2\psi + \Delta\varepsilon(90)\sin^2\psi \quad . \tag{21}$$

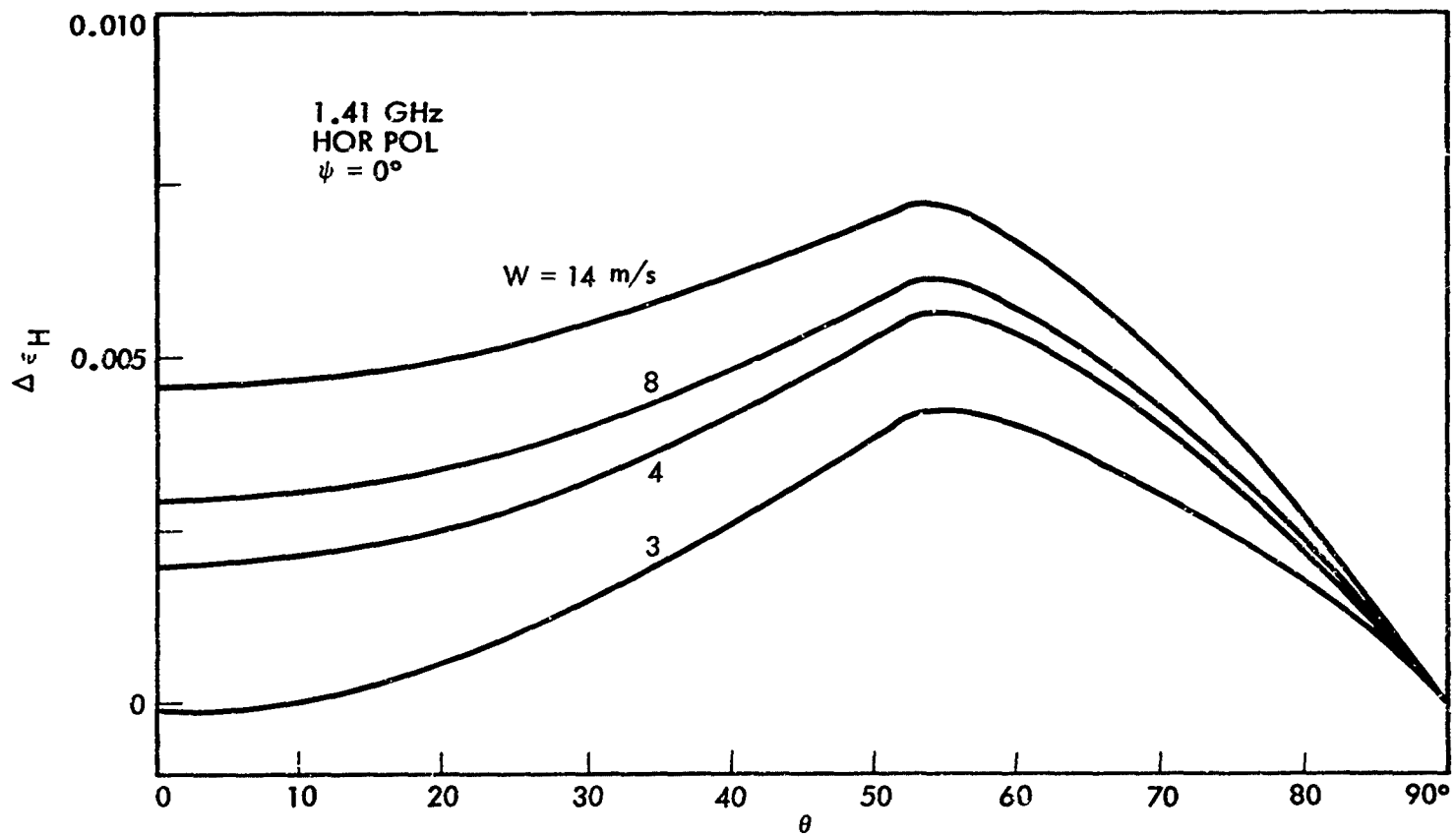

Fig. 1. Roughness dependence of the emissivity of a slightly rough surface. ν = 1.41 gHz, horizontal polarization, upwind observation.

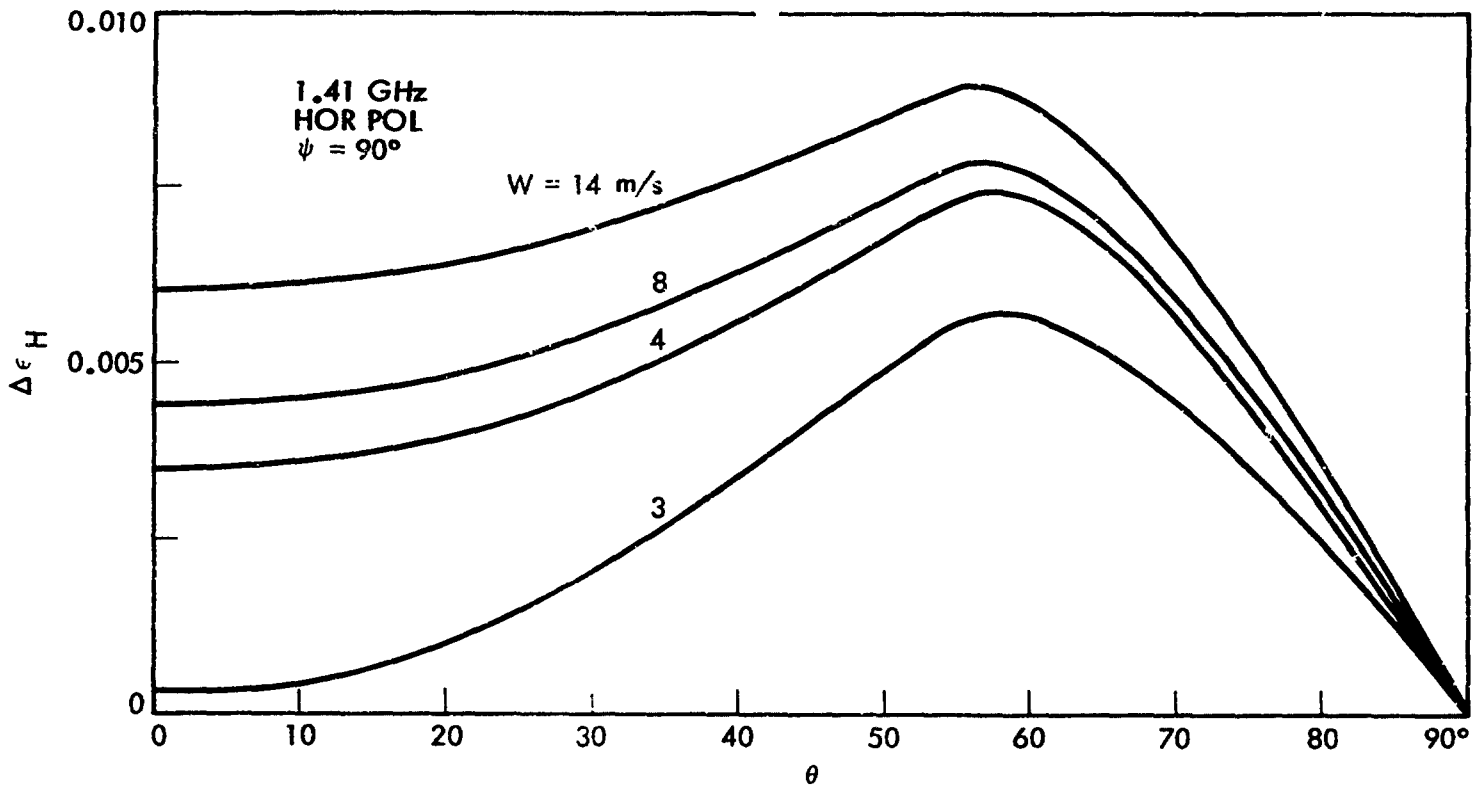

Fig. 2. Roughness dependence of the emissivity of a slightly rough surface. ν = 1.41 gHz, horizontal polarization, crosswind observation.

Unless otherwise indicated, the remaining figures will pertain to the case $\psi = 0°$. Figures 3 and 4 show the roughness effect for H polarization at frequencies of 8.34 and 14 gHz, and Fig. 5 that for 100 gHz. For 100 gHz, as stated earlier, the perturbation results may not be very accurate for $W \geq 14$ m/s; nevertheless, it is worth noting that the curves, at least to the left of the peak, are essentially the same as those given by the geometrical optics theory for the same surface. The dependence on frequency is shown in another way in Fig. 6 for a fixed observation angle of $\theta = 55°$.

A more complicated behavior is demonstrated by the vertically polarized radiation, as is shown in Fig. 7 for a frequency of 8.34 gHz and winds of 4, 8, and 14 m/s. At large nadir angles the rough surface would appear to be much colder than the smooth surface. The roughness effects tend to increase with increasing frequency for vertical polarization also; in Fig. 8 is shown, on a different scale, the region $\theta \geq 50°$ for a frequency of 19.35 gHz. As in the geometrical optics case for vertical polarization there is a tendency for the emissivity to be insensitive to surface roughness for angles in the neighborhood of 60°.

For the shorter wavelengths the structure of the spectrum itself begins to have a more prominent effect on the emissivity. The peak in the capillary range is approximated by a discontinuity at $K = K_c$ so that as the wind speed increases the high frequency cutoff, K_ν, of the spectrum will lie first below, then above, the discontinuity; as a result the emissivity, obtained from an integral over the spectrum, will show a discontinuity in its derivative with respect to W when $K_\nu = K_c$, i.e., at $W \sim 8.25$ m/s. The occurrence of this effect may be seen, for example, in Fig. 4 which shows a relatively large change in $\Delta\varepsilon_H$ between wind speeds of 8 and 8.5 m/s. It is also evident from Fig. 9 which shows the roughness effect as a function of wind speed for fixed observation

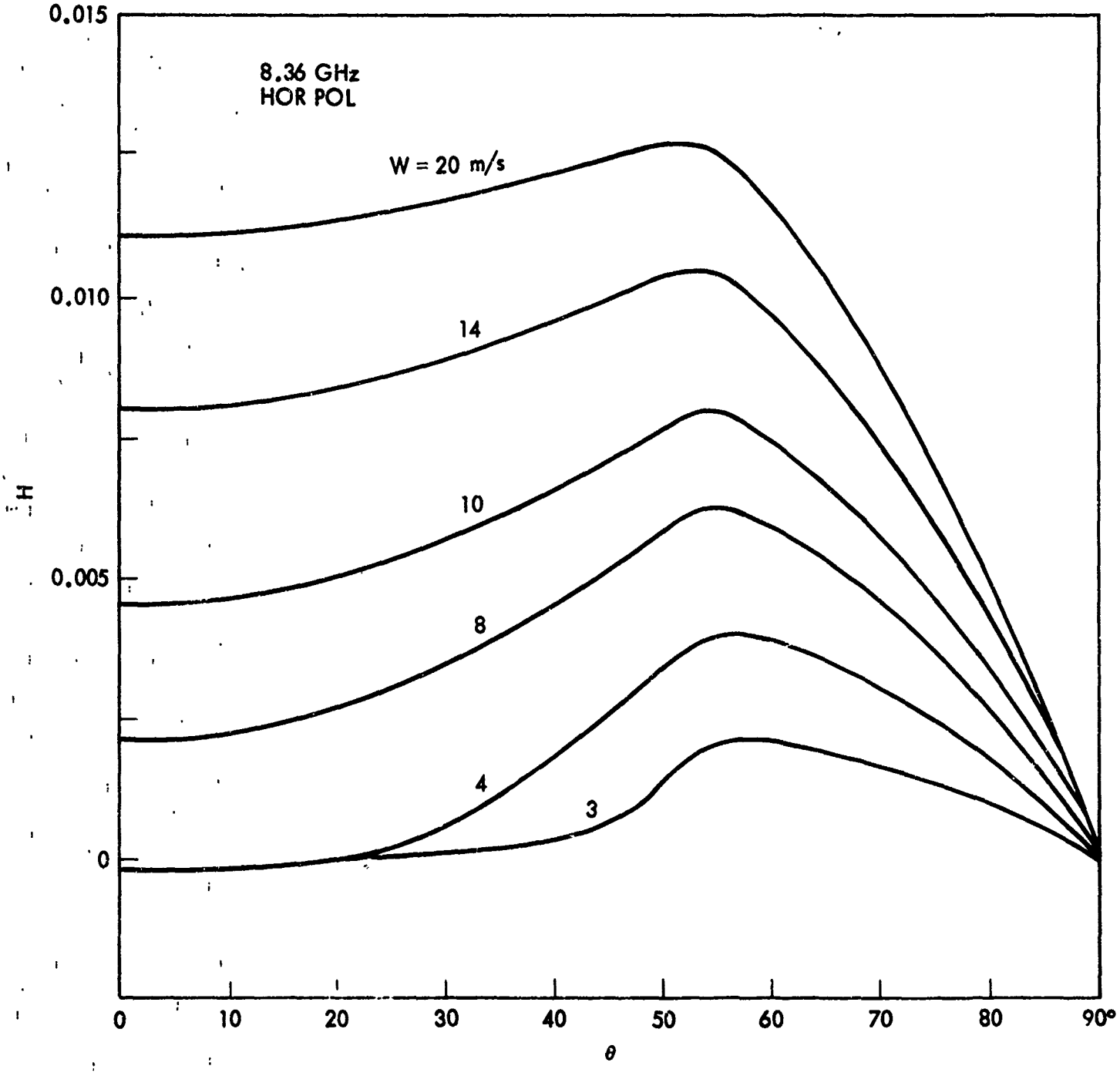

Fig. 3. Roughness dependence of the emissivity of a slightly rough surface. ν = 8.36 gHz, horizontal polarization.

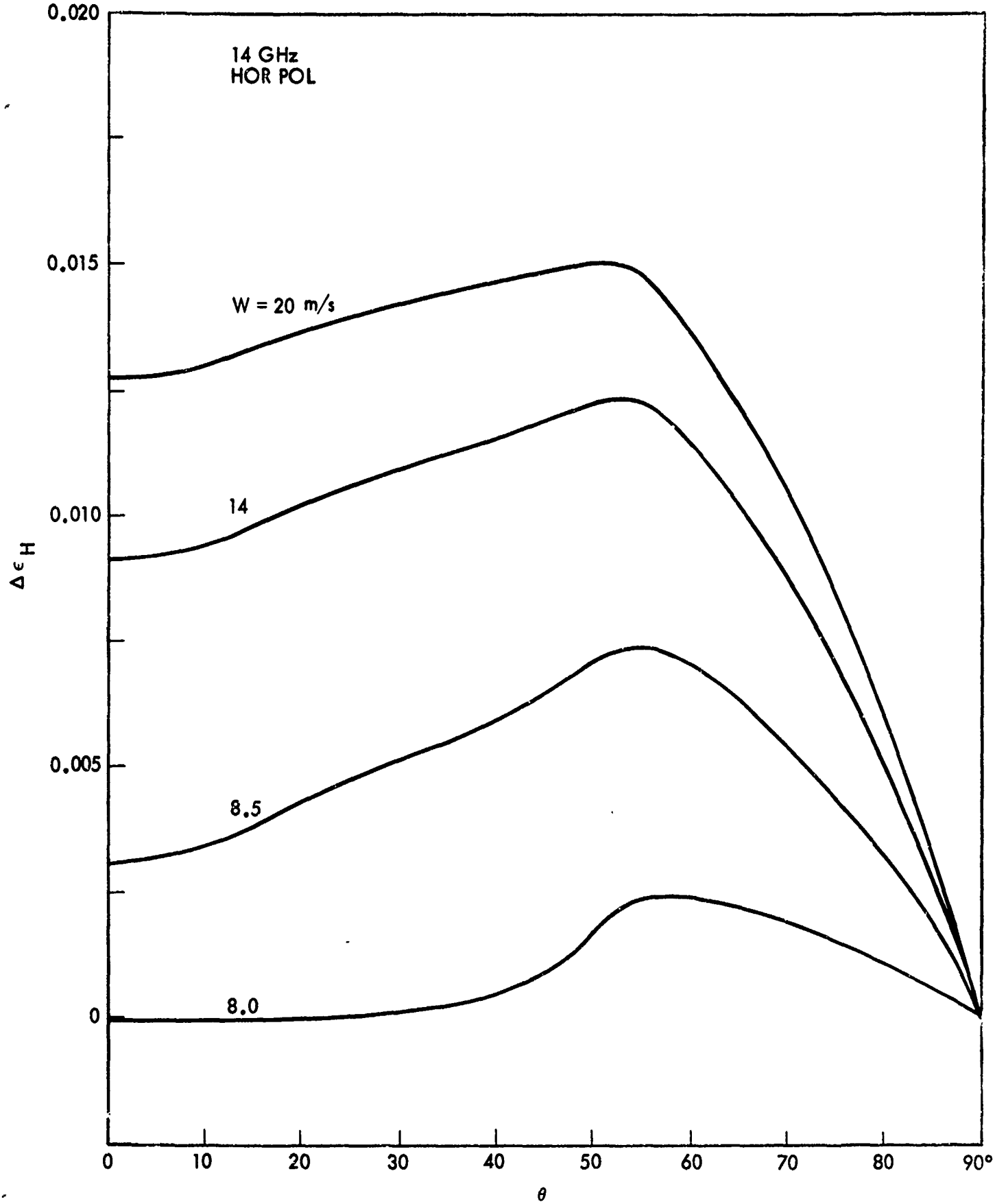

Fig. 4. Roughness dependence of the emissivity of a slightly rough surface. ν = 14 gHz, horizontal polarization.

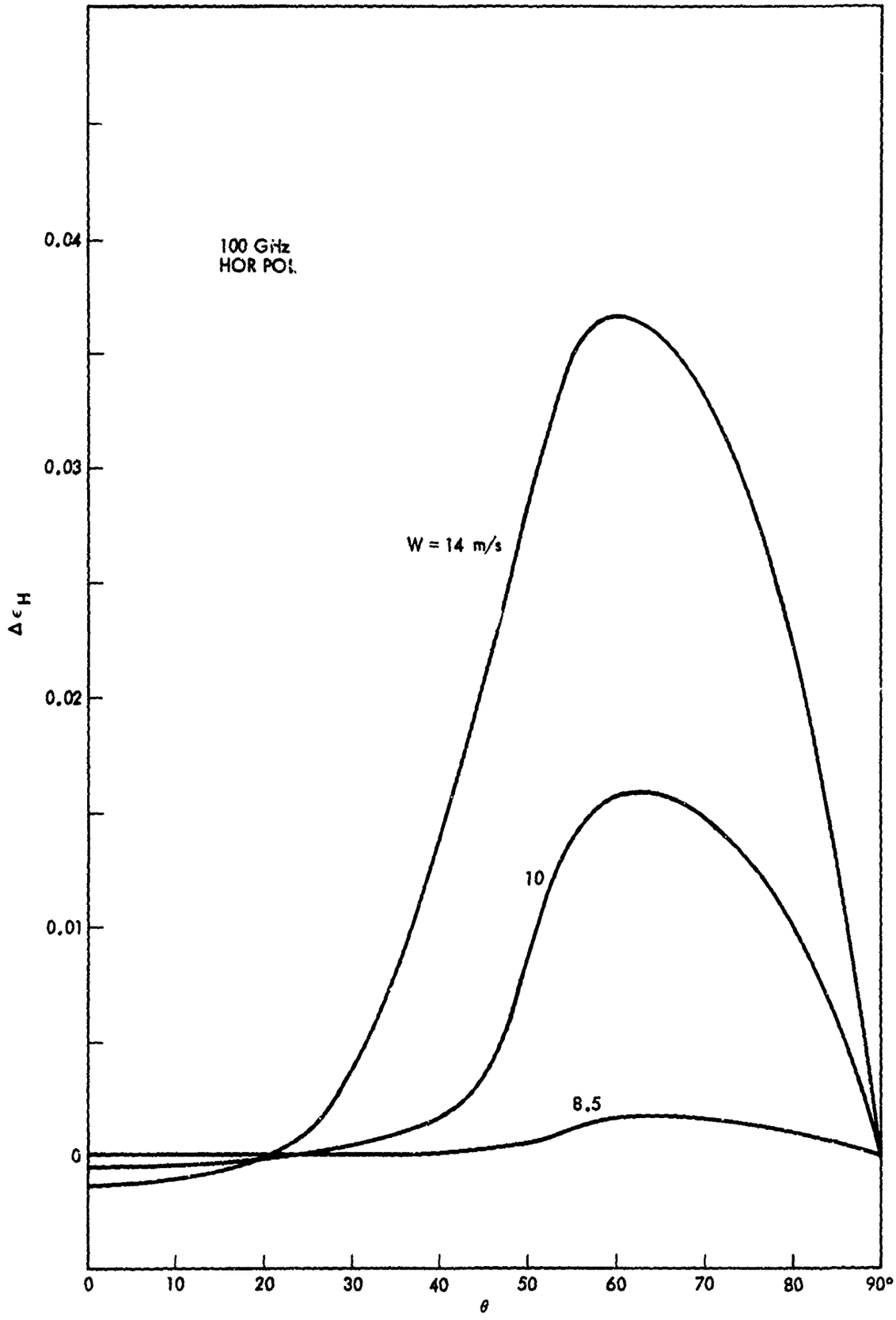

Fig. 5. Roughness dependence of the emissivity of a slightly rough surface. ν = 100 gHz, horizontal polarization.

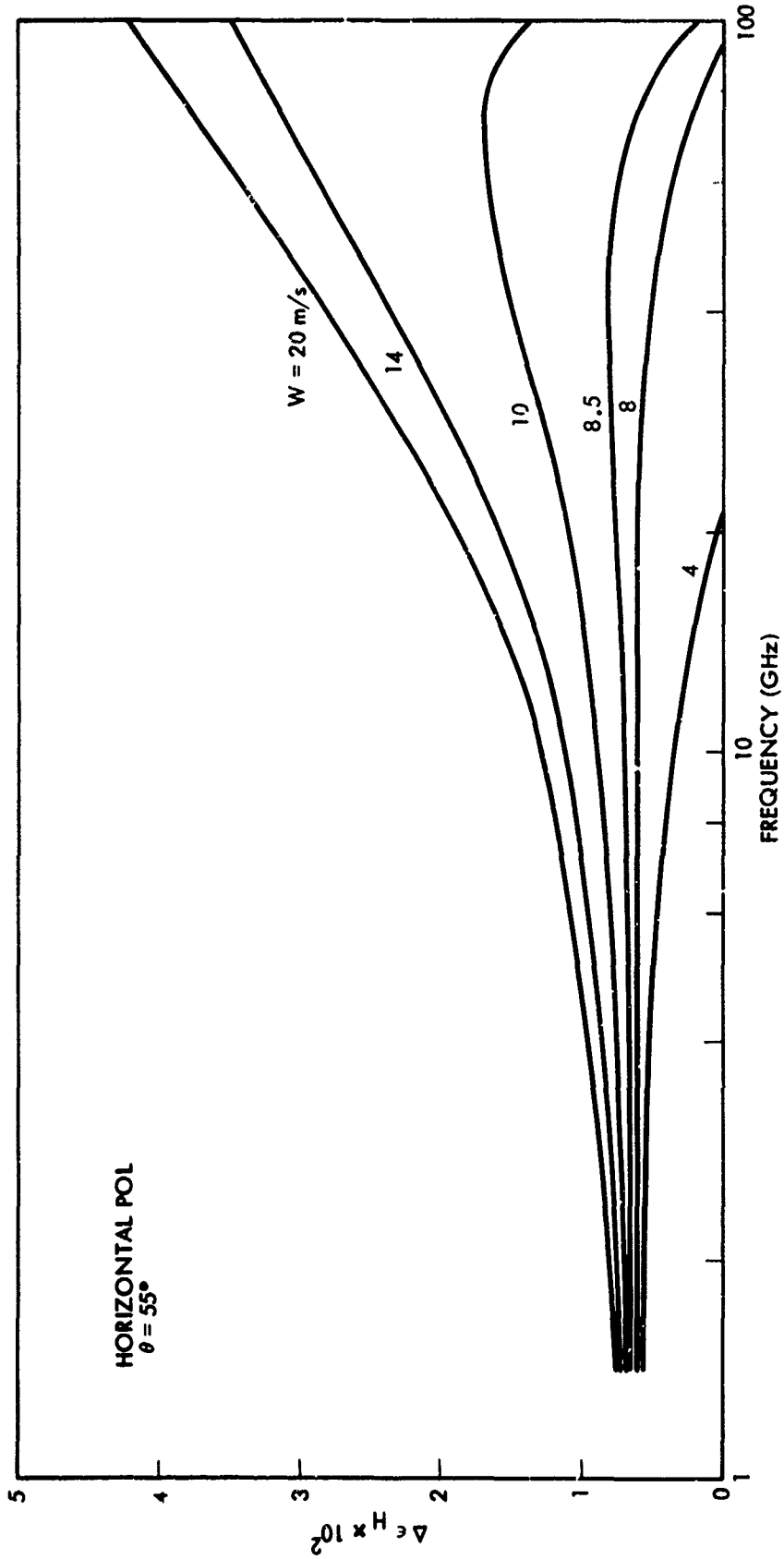

Fig. 6. Frequency dependence of the emissivity of a slightly rough surface at fixed observation angle and various wind speeds.

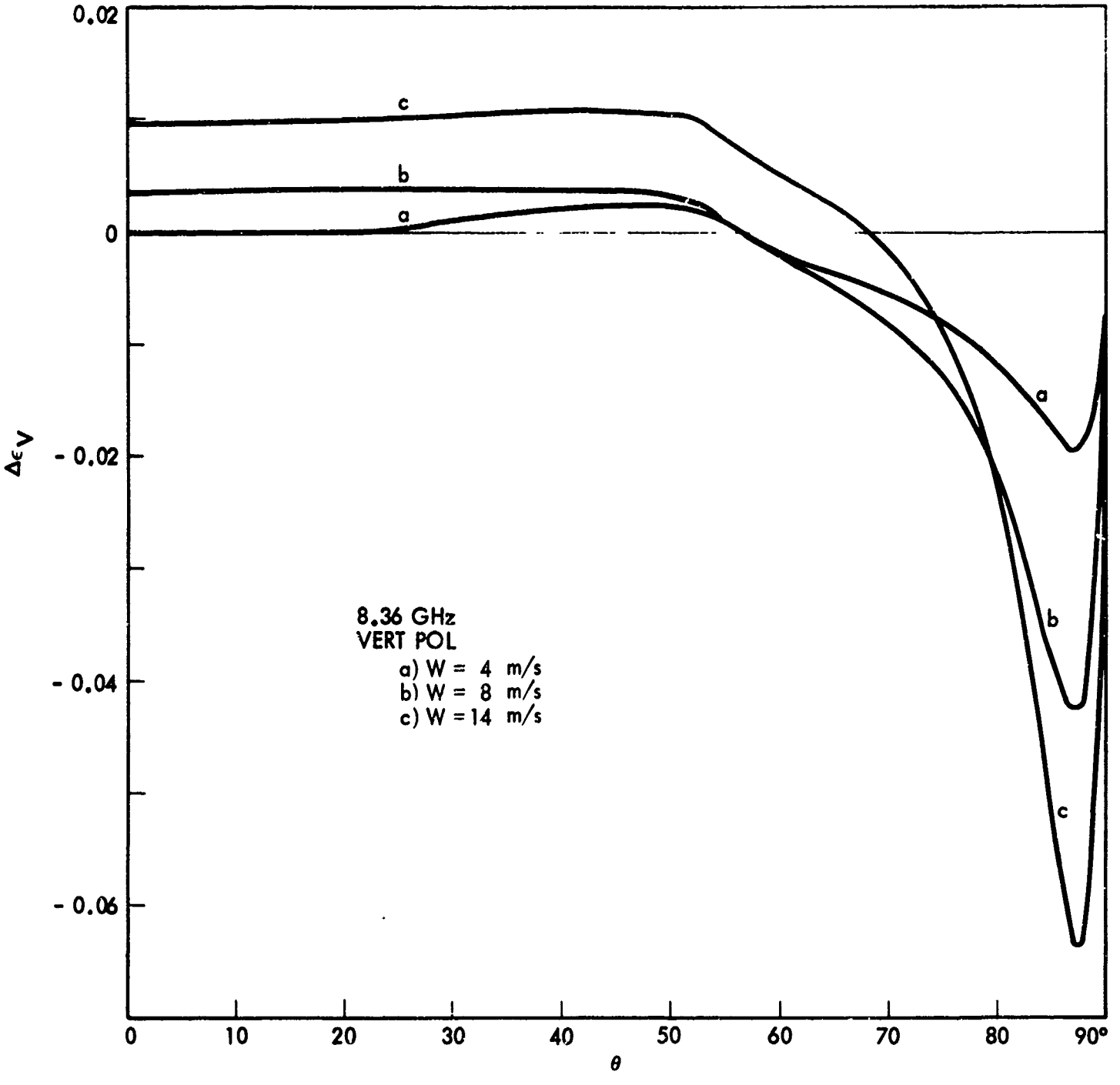

Fig. 7. Roughness dependence of the emissivity of a slightly rough surface. ν = 8.36 gHz, vertical polarization.

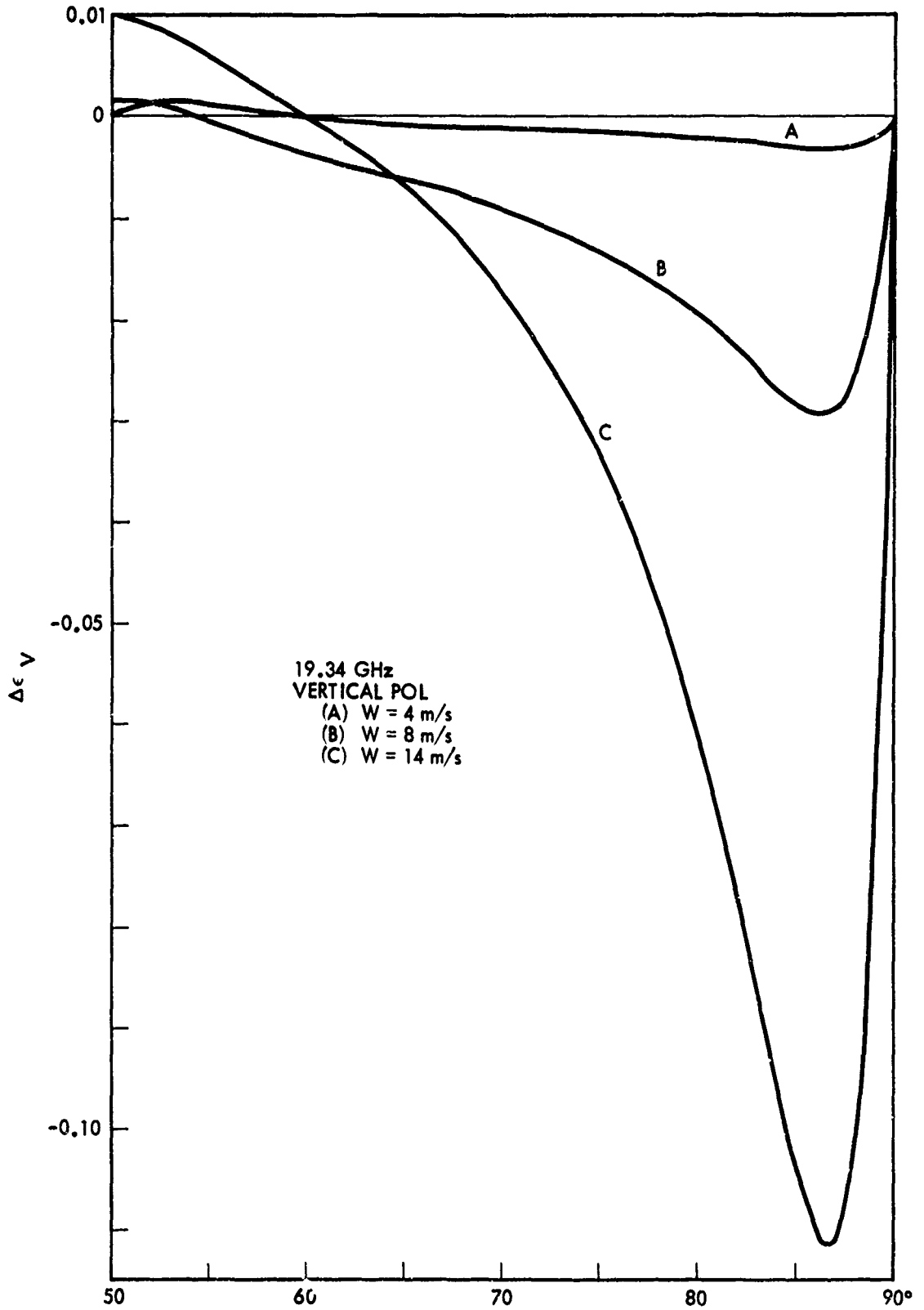

Fig. 8. Emissivity of small scale structure at large angles for 19.34 gHz, vertical polarization.

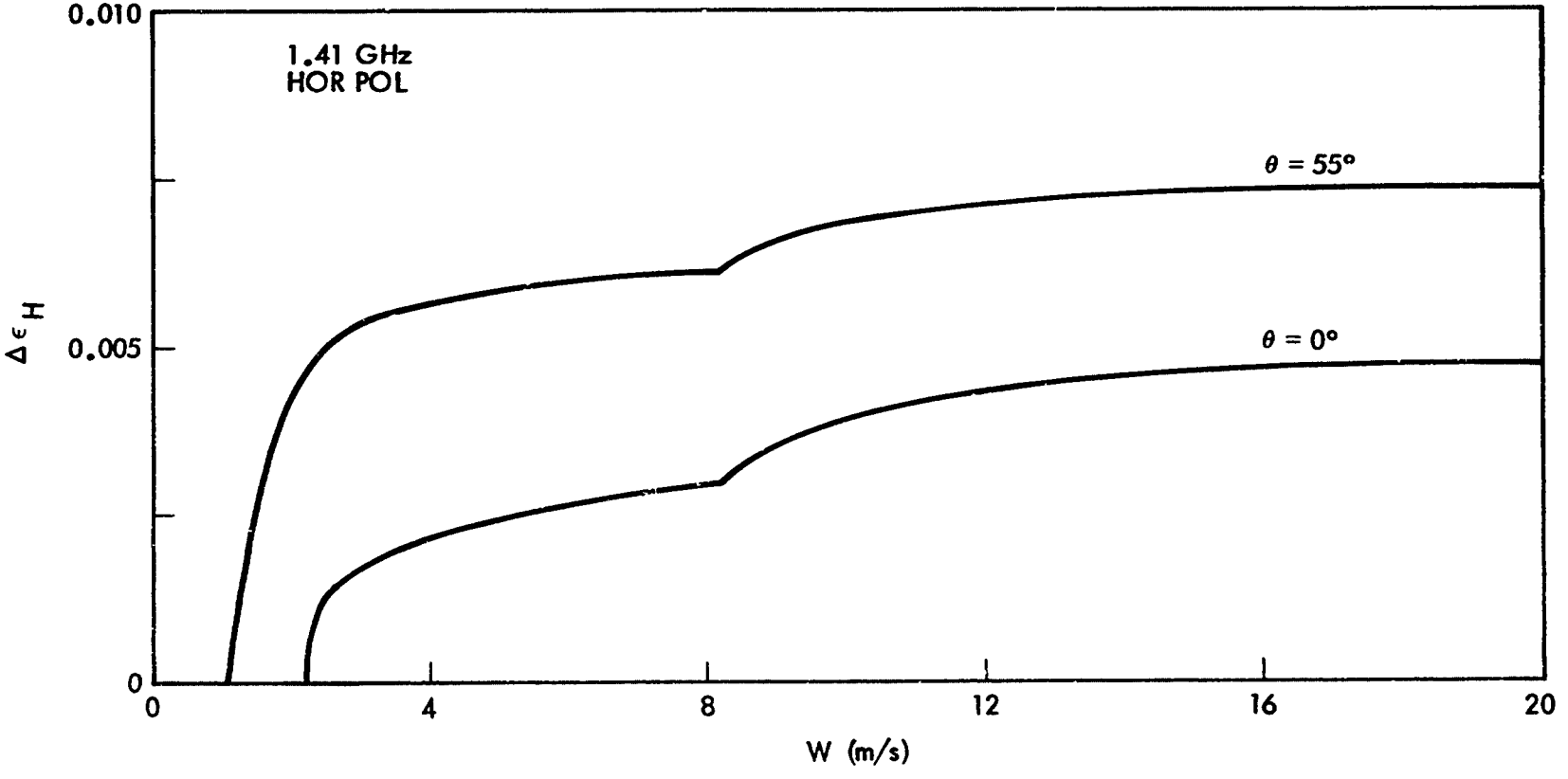

Fig. 9. Change in small-scale emissivity with wind speed, at fixed angle, illustrating the discontinuous derivatives resulting from discontinuities in the spectrum.

angles of $\theta = 0$ and 55°, at a frequency of 1.4 gHz and horizontal polarization. At very low wind speeds the rapid drop to zero of the curves in Fig. 9 is a consequence of the wind-speed dependent high frequency cutoff, K_ν, diminishing to the point where it is smaller than the low-frequency cutoff, 0.2k, assumed for the spectrum; the roughness effect is then identically zero. This, of course, is a direct result of our assumption of the existence of a low frequency cutoff for the small-scale spectrum and is not a real effect; in reality, the curves of Fig. 9 would presumably pass through the origin. We note that in the composite surface model this effect will not occur since the portion of the total spectrum excluded from the small scale spectrum (values of S(K) for K less than the smaller of 0.2k, K_ν) are automatically included in the large-scale spectrum.

Under certain conditions the discontinuities in the spectrum will also manifest themselves in the variation of $\Delta\varepsilon$ with θ, for fixed wind speed. To show this we note that, for a given frequency and wind speed, the integrations over the two-dimensional spectrum in the emissivity equations (given in the Appendix) extend over a fixed annular region of K_x, K_y space. However, in these equations the spectrum is not centered at the origin but is displaced from it by an amount which increases with θ and k. Thus as θ increases from 0° a circle of discontinuity moves across the $\underline{K}$ plane and eventually intersects the integration annulus and, as θ increases further, passes on through. The emissivity will show an effect of a discontinuity in the spectrum for that range of θ for which an intersection exists between the circle and the integration annulus. This is illustrated in Fig. 10 which shows $\Delta\varepsilon_v$ vs. θ at a frequency of 19.35 gHz. The hump in the curves at small angles can be traced to the discontinuity at $K = K_\nu$ associated with the onset of the capillary range. At the low wind speed of 4 m/s the discontinuity having the principal effect is

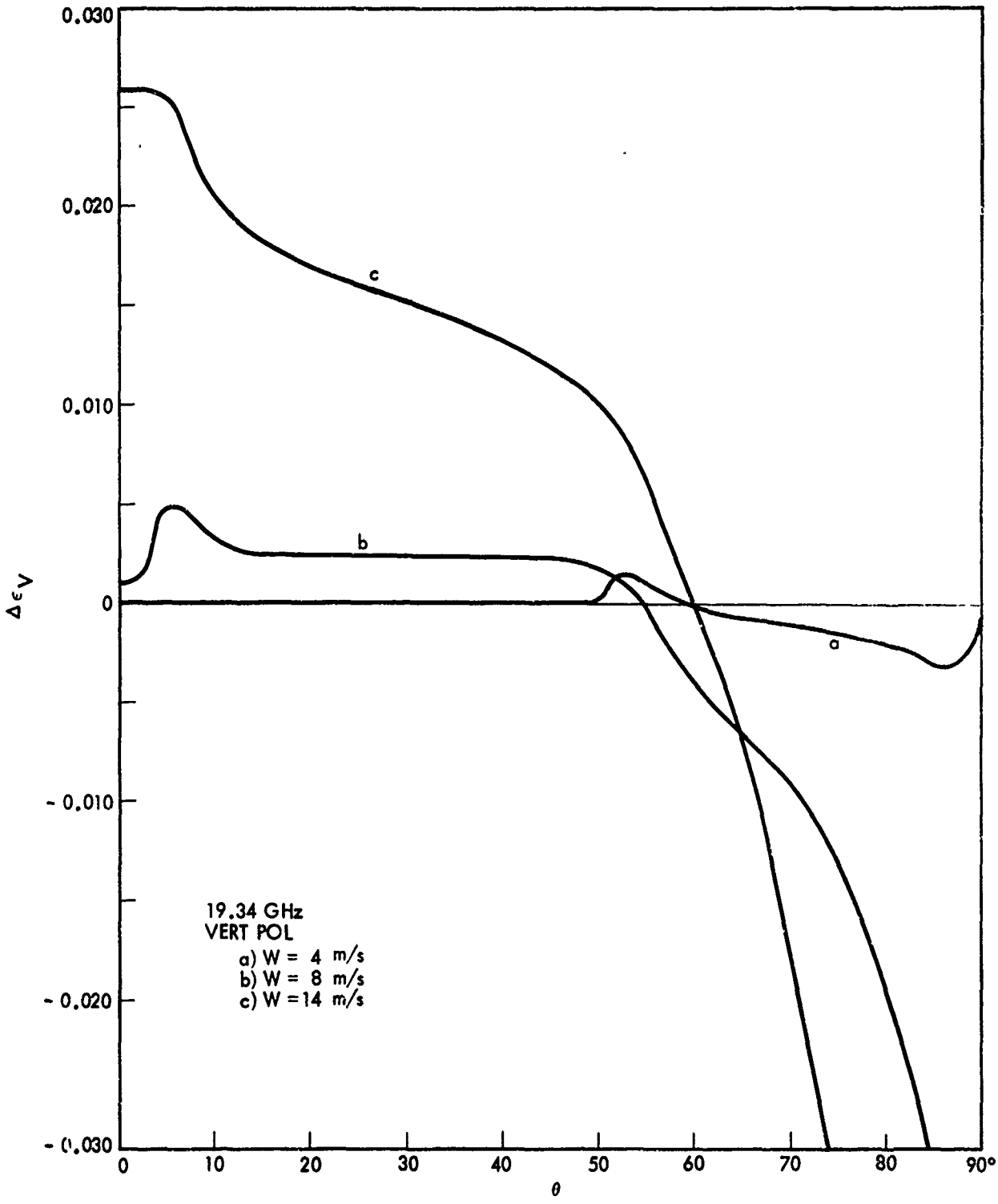

Fig. 10. Angle dependence of the small-scale emissivity at 19.34 gHz, vertical polarization. The small peaks result from discontinuities in the spectrum.

that at K_v; it occurs at larger values of θ in this instance and produces a small peak at $\sim 55°$. For $\theta \lesssim 50°$ there is no contribution of roughness to the emissivity since the spectrum, in this particular case, will not overlap the integration annulus. To what extent these effects are model-dependent is not known but should be investigated; in any case, they appear to be small and will produce a variation in apparent emission temperature of less than 1°K.

IV. SEA BRIGHTNESS TEMPERATURES

Before applying and using any model it is advisable to test it for internal consistency. A necessary condition for the validity of a scattering or emission theory is that it conserve energy. It has been shown[4,5] that an equivalent condition is that the emissivity of the emitting surface go to zero as the conductivity of the medium becomes infinite. This condition is always satisfied for the direct emission method since the emissivity of every surface element (i.e., the emissivity of a slightly rough surface) may be shown to be zero for a perfect conductor. While the composite surface model using the Peake representation was not used for emissivity calculations, except for purposes of comparison, essentially the same model was used to evaluate the scattered atmospheric radiation. Calculating the emissivity of a perfect conductor leads to the results shown in Fig. 11 [curves a.) and b.)] for a frequency of 1.4 gHz and a wind speed of 14 m/s. The results are quite good with the maximum departure from exact energy conservation being 0.015 for the scattering model. For comparative purposes, the result for the purely geometrical optics model is shown in curve c.). (The corresponding calculation using the non-energy-conserving Stogryn theory was reported earlier.)[3]

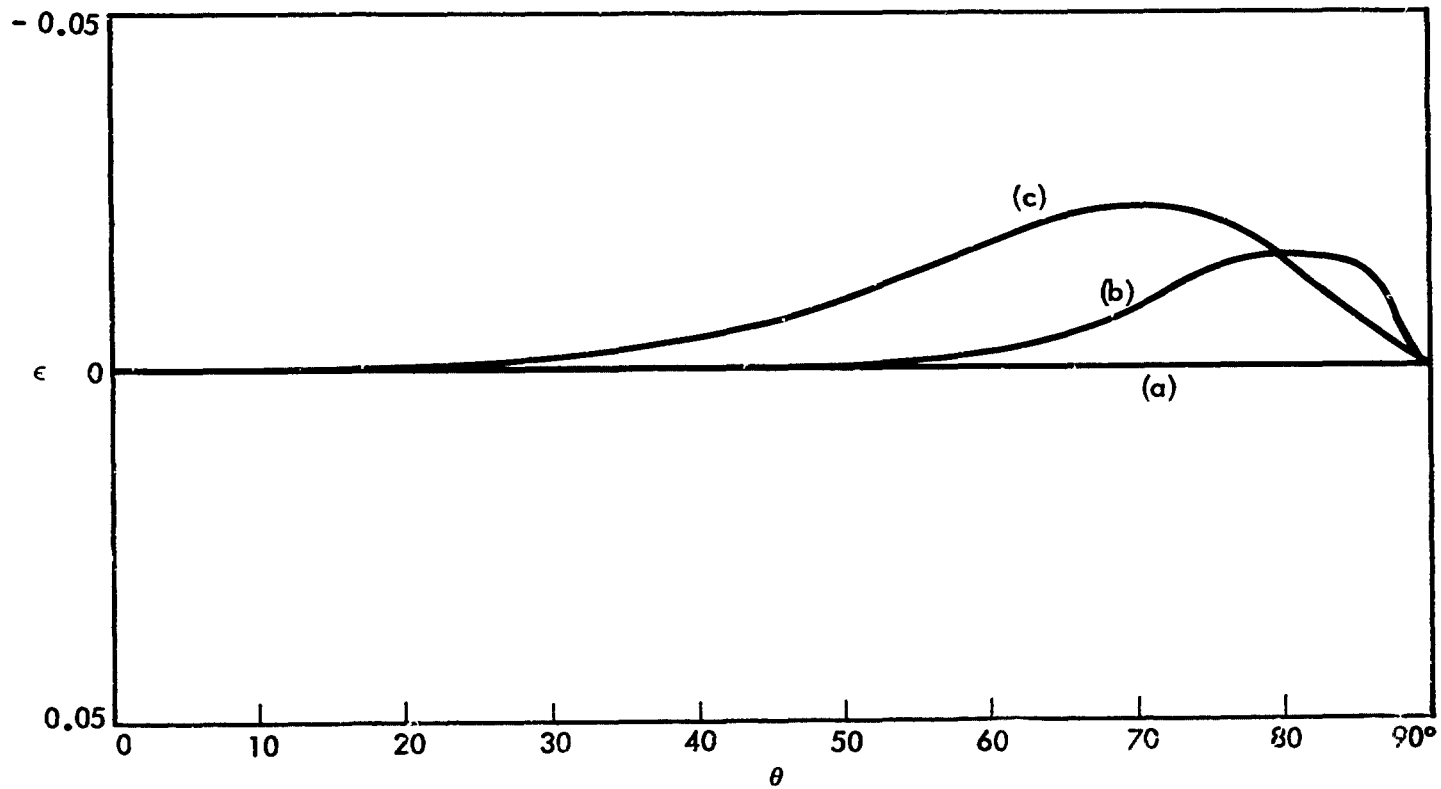

Fig. 11. Emissivity of a perfectly conducting sea surface (energy conservation), calculated for a) composite surface, direct emission method, b) composite surface, Peake integral method, c) geometrical optics model. A frequency of 1.41 gHz and wind speed of 14 m/s are assumed. The correct result is $\varepsilon \equiv 0$.

Two other results concerning the relationship between the direct emission method and Peake integral method are of interest. First, as in the geometrical optics model, the higher-order multiple scatter contributions to the emissivity were found to be an order of magnitude larger (for H polarization) in the Peake method than in the direct emission method, implying a correspondingly greater sensitivity to approximations which must necessarily be made in the difficult calculations of the higher-order effects. Secondly, it was proved theoretically for the purely geometrical optics theory that the Peake method gave an upper bound to the effects of surface roughness on the emissivity while the direct emission method gave a lower bound.[5] Surprisingly, the same relationship between the emissivities calculated numerically by the two methods was also found to hold, without exception, in the composite surface model. Whether the existence of the bounds in the present model is simply a consequency of the specific details ascribed to the model, or whether the proof of the existence of the bounds is actually valid outside the domain of geometrical optics, is not known at this time.

The roughness parameter in the geometrical optics theory is the rms slope of the entire sea surface, as given by the Cox and Munk equations, while for the large-scale component in the composite model it is the rms slope of the large structure alone. From the definition of the large-scale spectrum it is evident that as the frequency decreases the rms slope will steadily decrease from the Cox and Munk value. The dependence of the large-scale rms slope on wind speed is shown in Fig. 12 for frequencies of ∞, 100, 19.35, and 1.4 gHz. At low wind speeds there is little difference in the wind speed dependence except for the lowest frequencies. At W = 14 m/s, the rms slope at 19 gHz is about 0.67 of its geometrical optics value while at 1.4 gHz the ratio is $\sim$0.55.

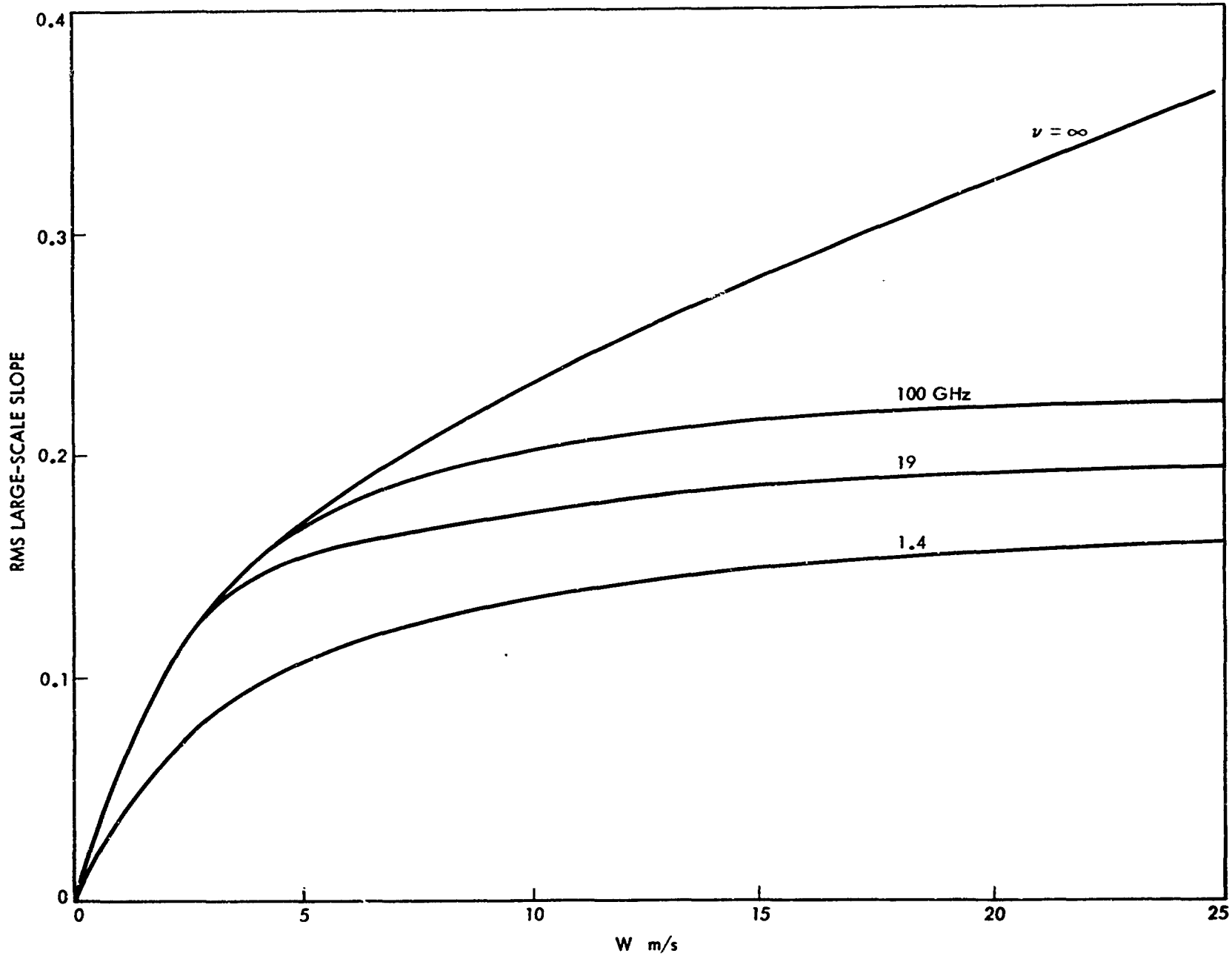

Fig. 12. Root mean square slope of large-scale sea roughness as a function of wind speed and frequency.

If the small-scale roughness had no effect whatever on the emissivity, then the frequency dependence of the brightness temperature would be described by Fig. 12. That is, the microwave sea brightness temperature would be accurately described by the purely geometrical optics model but with an effective rms slope given, at a particular frequency and wind speed, by Fig. 12. As will be seen later, this is approximately what does in fact occur, at least at the lower frequencies where the effect of the small structure is not large. At 19 gHz the reduction in the large-scale slope (from the geometrical optics value) tends to be compensated for by an increased effect of the small-scale structure so that the net departure of the brightness temperature from the purely geometrical optics result is not large.

Sea brightness temperatures were calculated numerically for 6 frequencies between 1.4 and 19.35 gHz water temperatures of 283, 293, and 298°K, various salinity values between fresh and very saline, and atmospheric humidity values corresponding to dry, average, and humid atmospheres. The dependence on all the parameters except frequency, polarization, and wind speed differ only in negligible detail from that given by the geometrical optics model. Since these have already been reported[6] we shall here be concerned only with the dependence on those parameters for which the brightness temperature shows a significant departure from the geometrical optics results.

All the values quoted in the remainder of this report refer, unless stated otherwise, to the case of an atmosphere of average humidity, water temperature of 20°C, salinity of 35 ppt, and a plane of observation parallel to the wind direction. Since it is not possible to present, even in summary form, the results of all the computations at all frequencies, only selected results at those frequencies for which data is available will be considered.

Figures 13 - 18 show the dependence of the sea brightness temperature on observation angle for various wind speeds, at frequencies of 1.41, 8.36, and 19.34 gHz and both polarizations. Comparing with the corresponding figures for the geometrical optics model we see that there is no qualitative difference between the behavior predicted by the composite surface and geometrical optics models, except perhaps for an increased sensitivity to wind speed at 19.34 gHz for wind velocities greater than 8 m/s. A detailed comparison between the two models is shown in Figs. 19 - 30 for the same frequencies and polarizations and wind speeds of 8 and 14 m/s. Except possibly for large observation angles, the composite surface model predicts brightness temperatures which are somewhat larger than those calculated with the geometrical optics model; the difference is about 1°K at the lower frequencies up to about 4°K at the highest frequency. It may be shown that at the low frequencies the reduction in the rms slope (from the g.o. value) associated with the large-scale roughness component has a negligible effect on the brightness temperature (except at very large angles) while the small-scale component adds a small (generally positive) contribution. For vertical polarization and large angles there is a competition between a decrease in the emissivity due to the small-scale structure (cf. Sect. III) and an increase due to the effect of the reduced large-scale slope on both the emissivity and reflected atmospheric radiation. One would expect that if the angle dependence of the diffusely scattered sky radiation were explicitly taken into account (cf. Sect. II), the brightness temperatures at nadir would increase further, due to the large-angle scattering of radiation from the hotter regions of the sky, while those near the horizon would be reduced; this effect is not expected to be large, however.

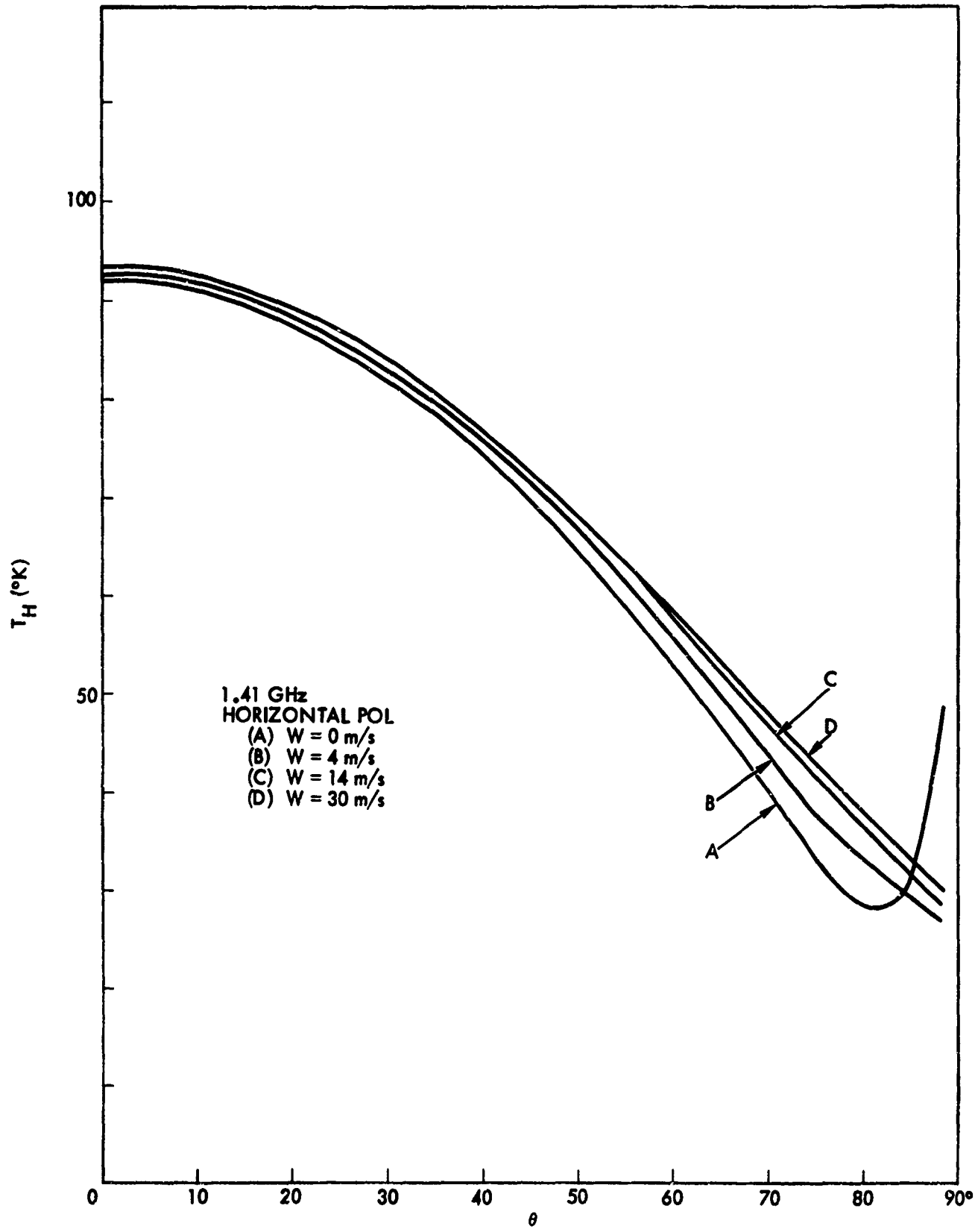

Fig. 13. Horizontally polarized sea brightness temperatures at 1.41 gHz.

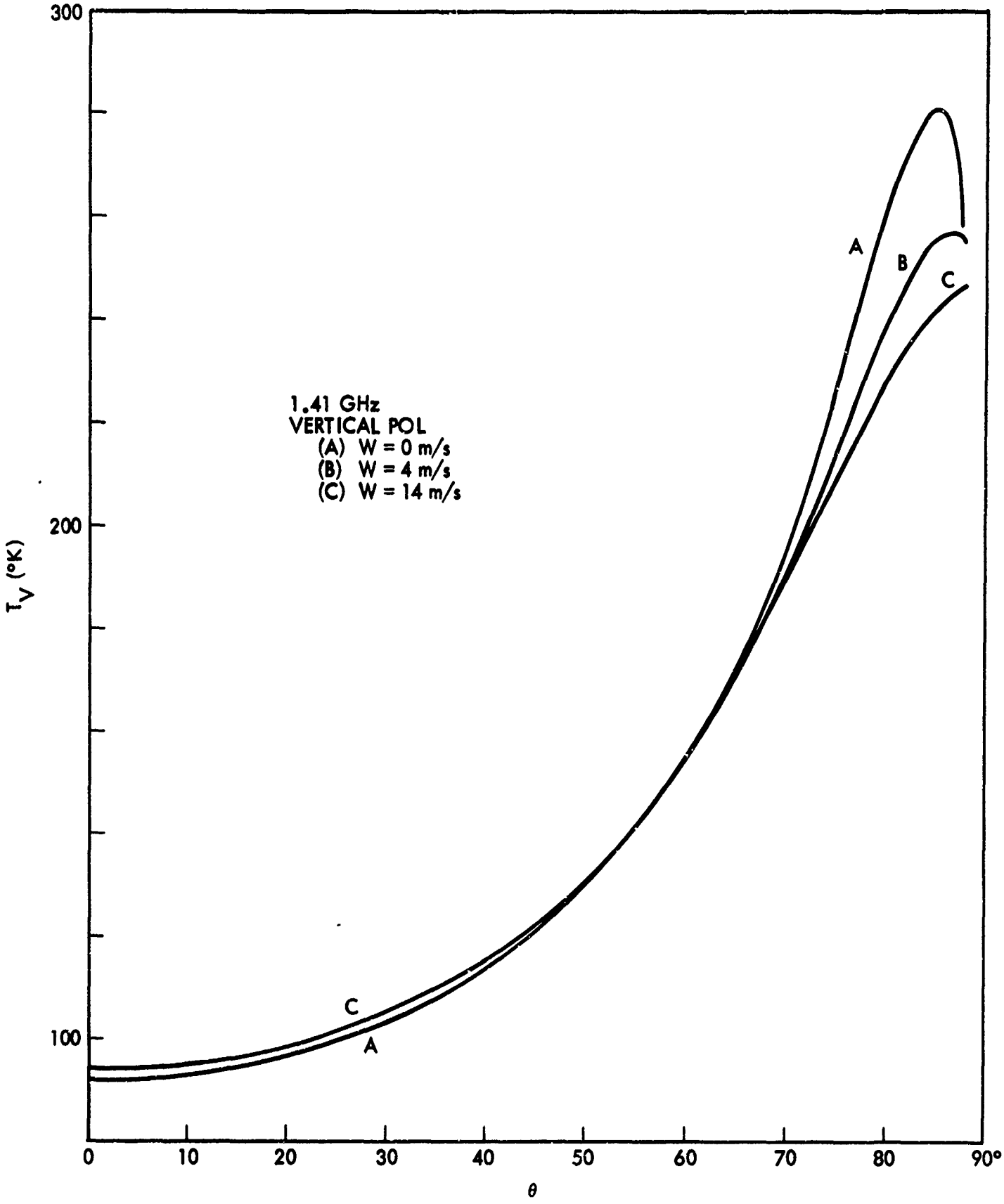

Fig. 14. Vertically polarized sea brightness temperatures at 1.41 gHz.

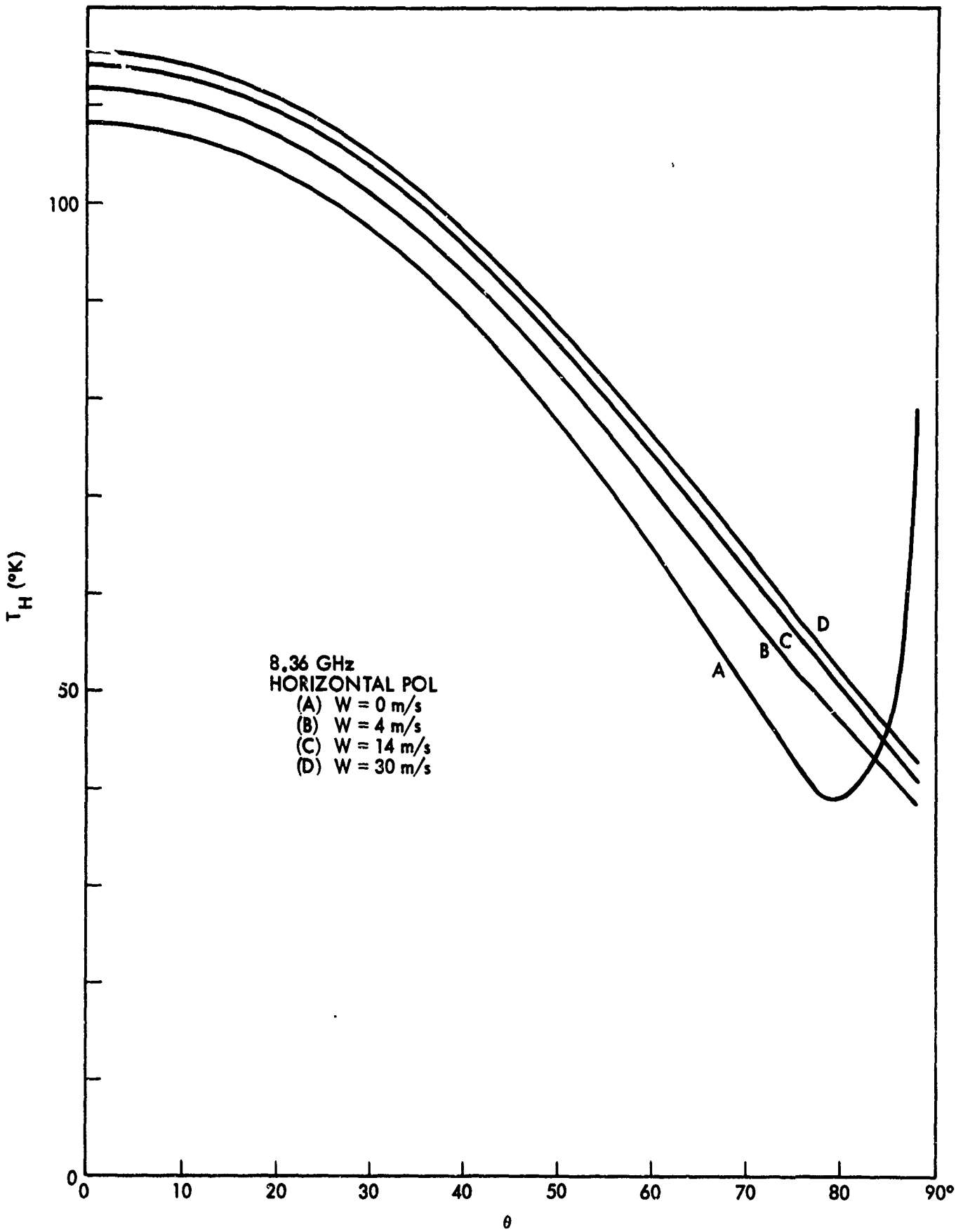

Fig. 15. Horizontally polarized sea brightness temperatures at 8.36 gHz.

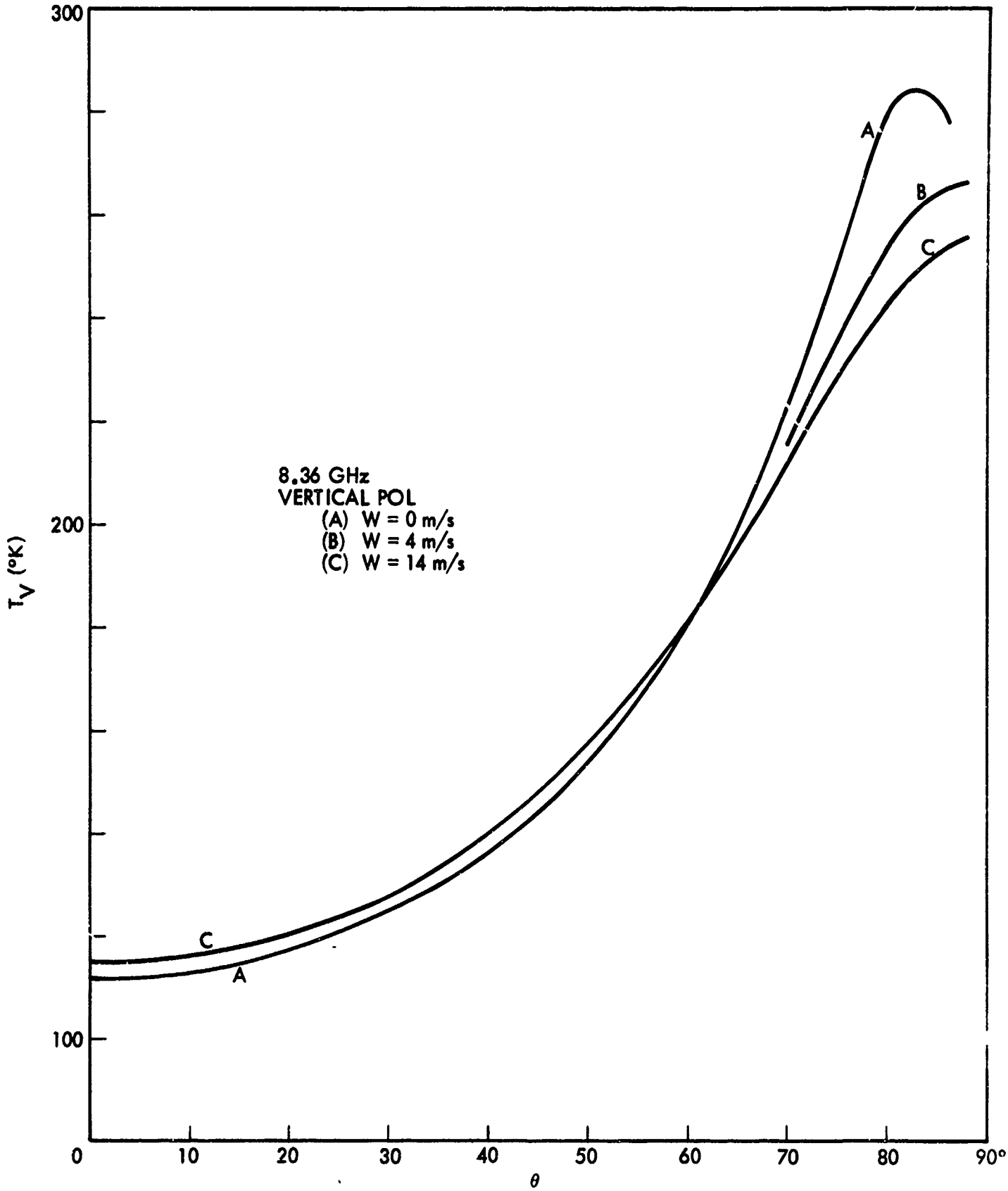

Fig. 16. Vertically polarized sea brightness temperatures at 8.36 gHz.

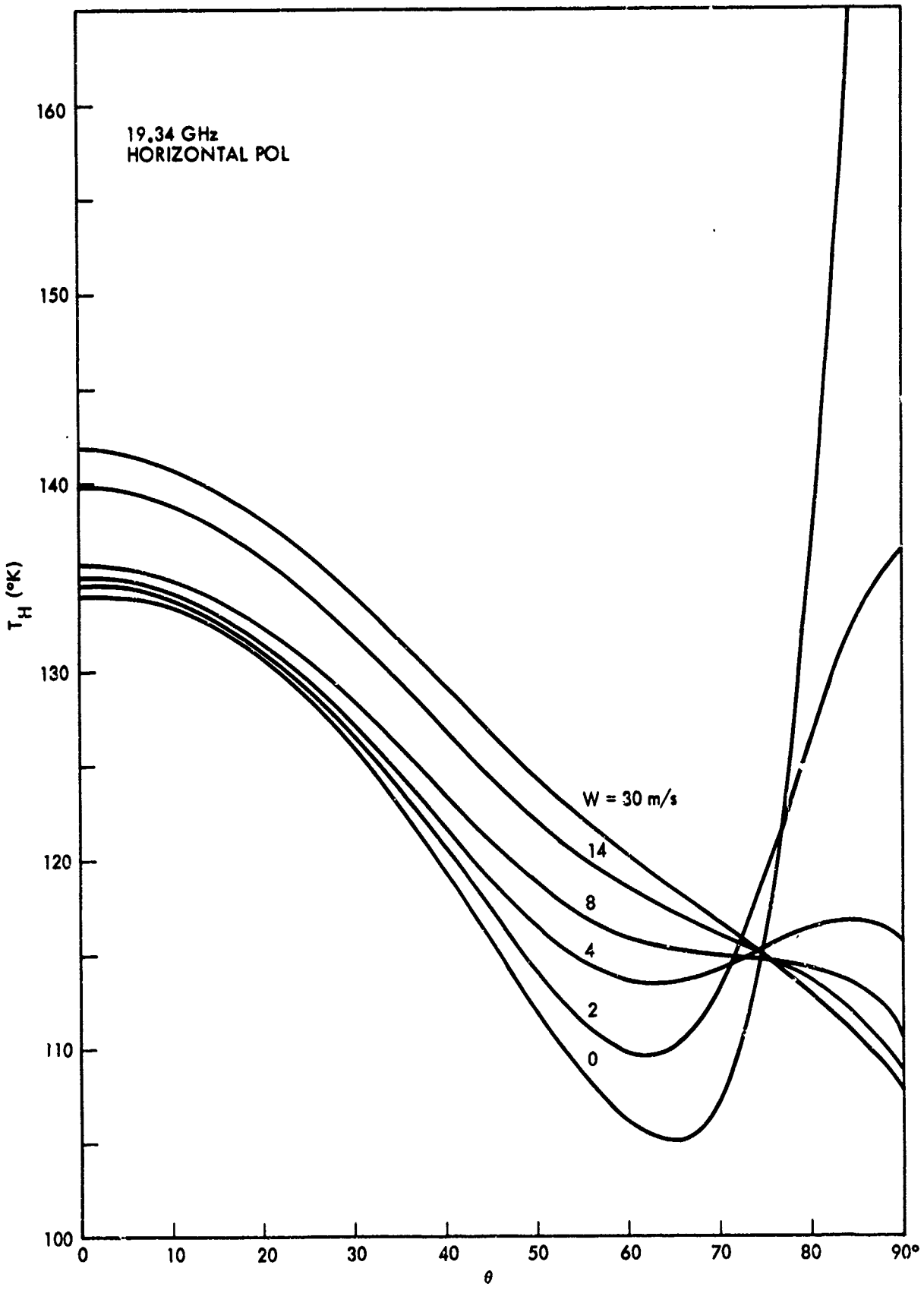

Fig. 17. Horizontally polarized sea brightness temperatures at 19.34 gHz.

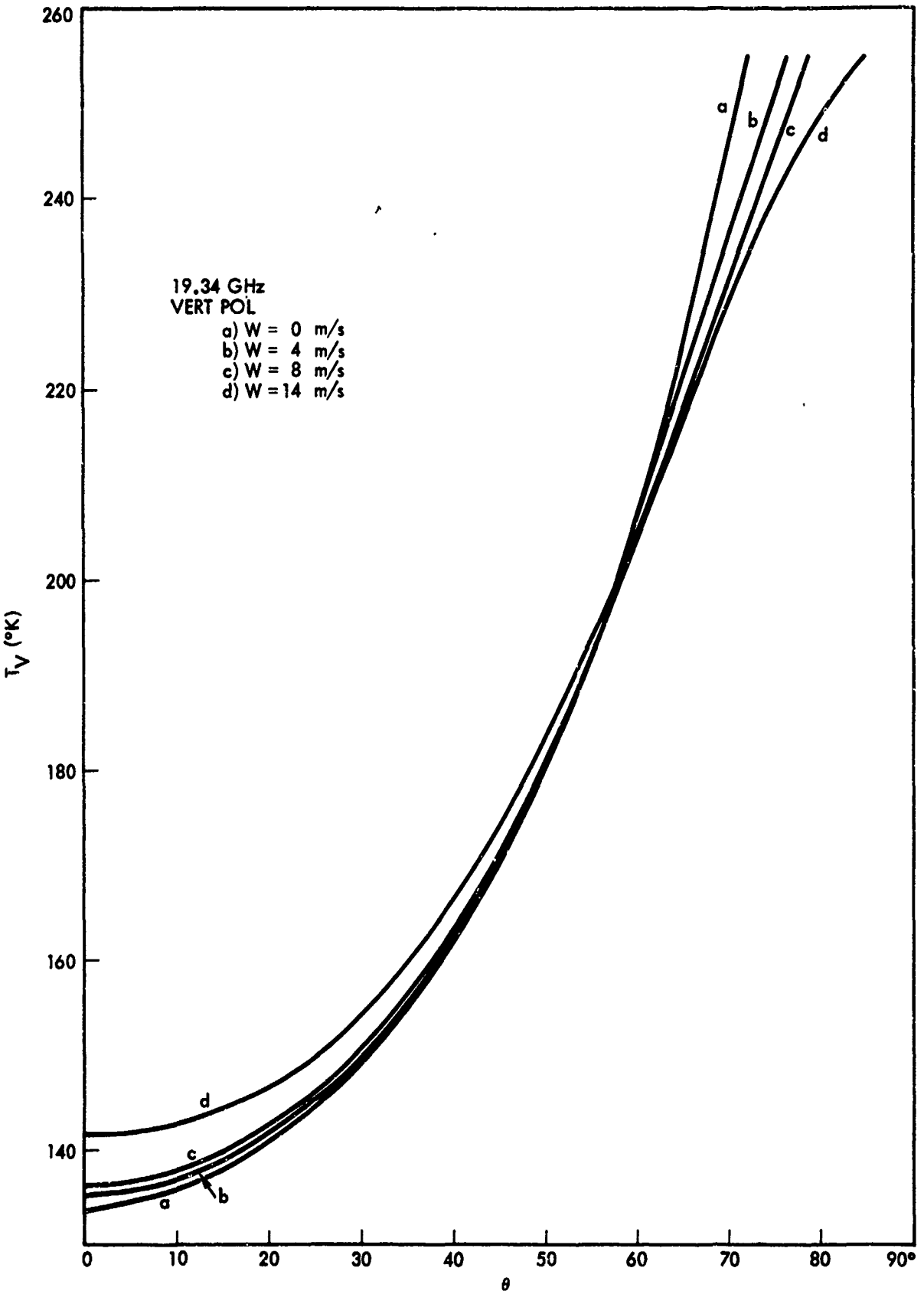

Fig. 18. Vertically polarized sea brightness temperatures at 19.34 gHz.

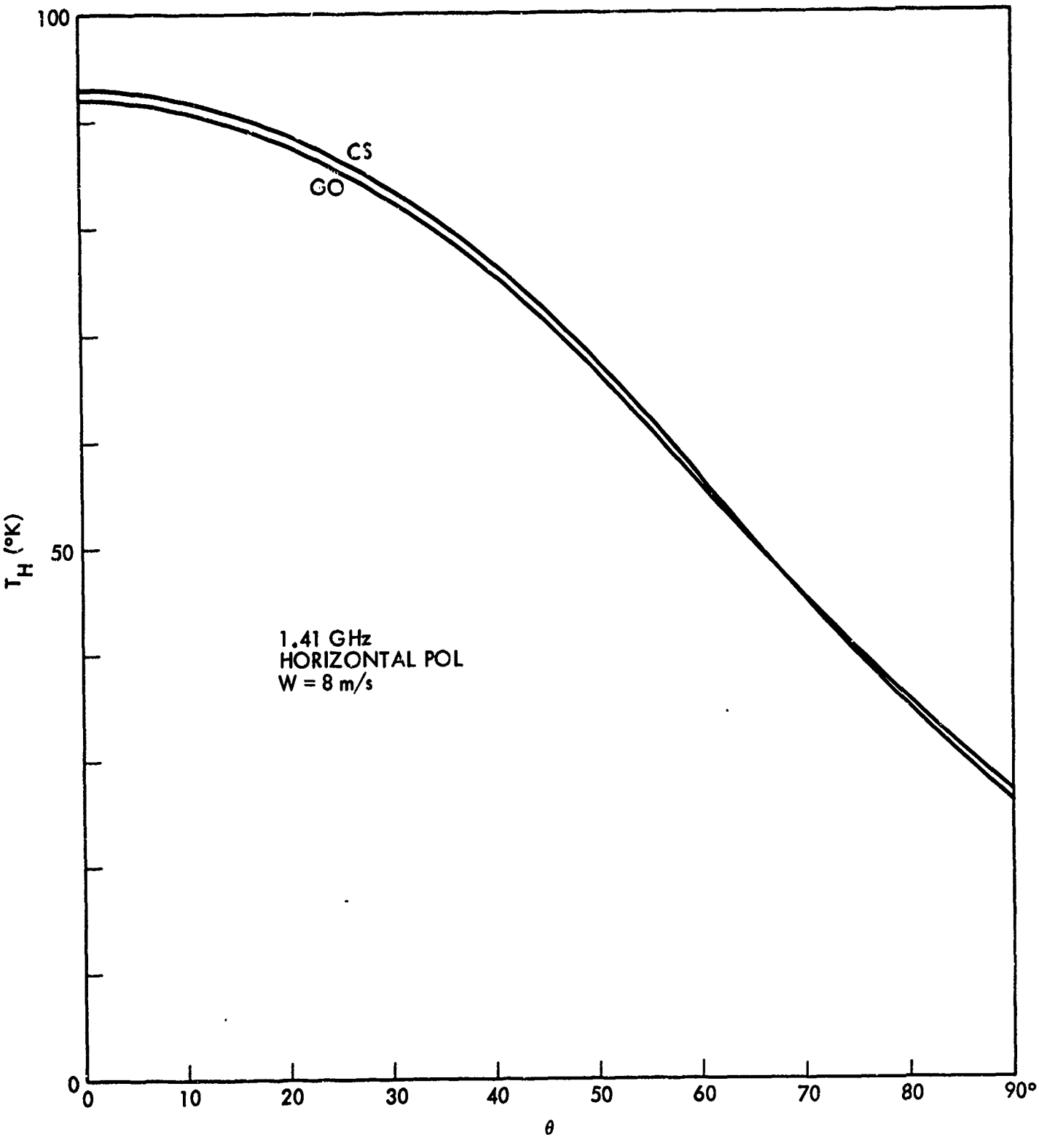

Fig. 19. Comparison of composite surface and geometrical optics brightness temperatures.

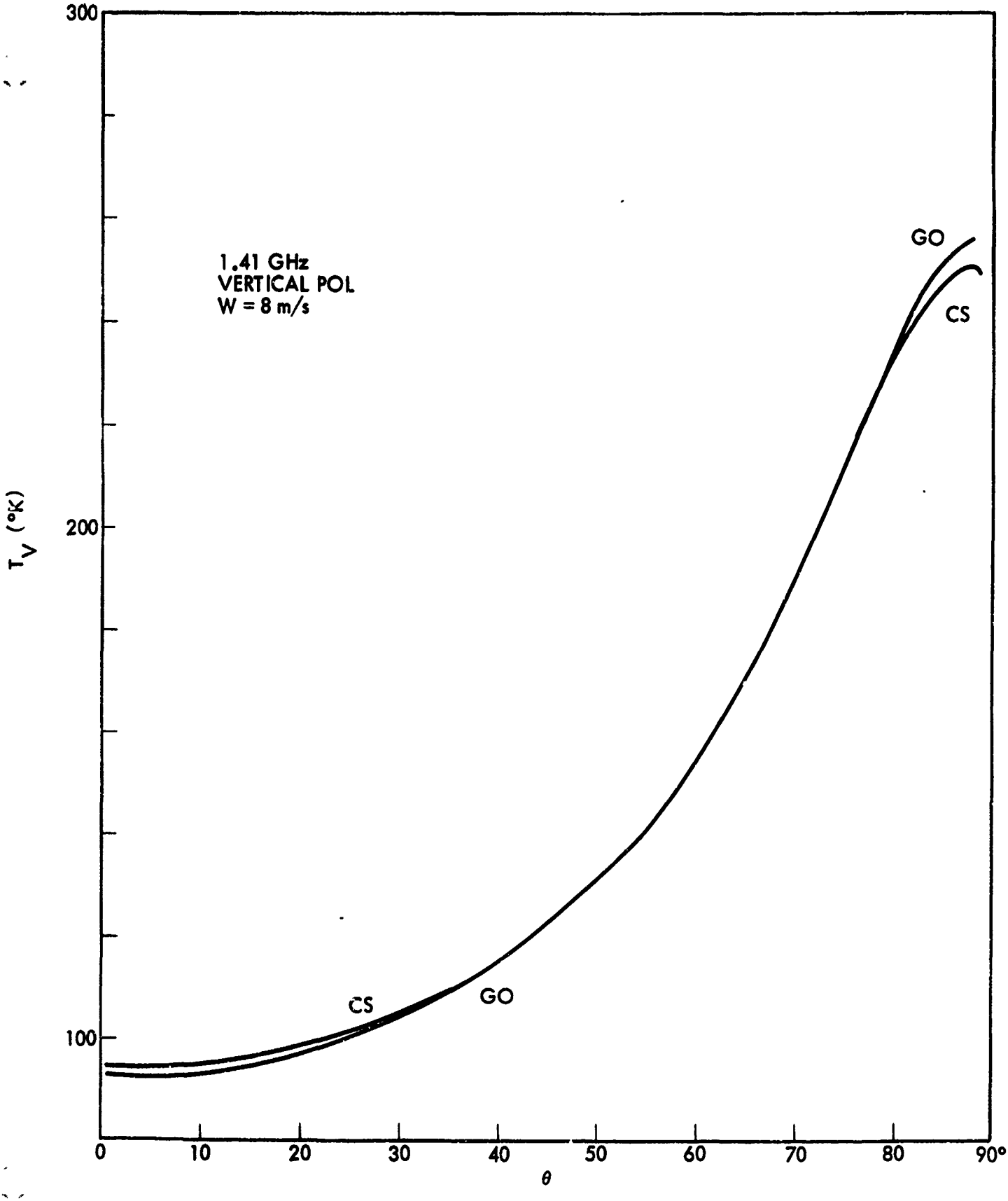

Fig. 20. Comparison of composite surface and geometrical optics brightness temperatures.

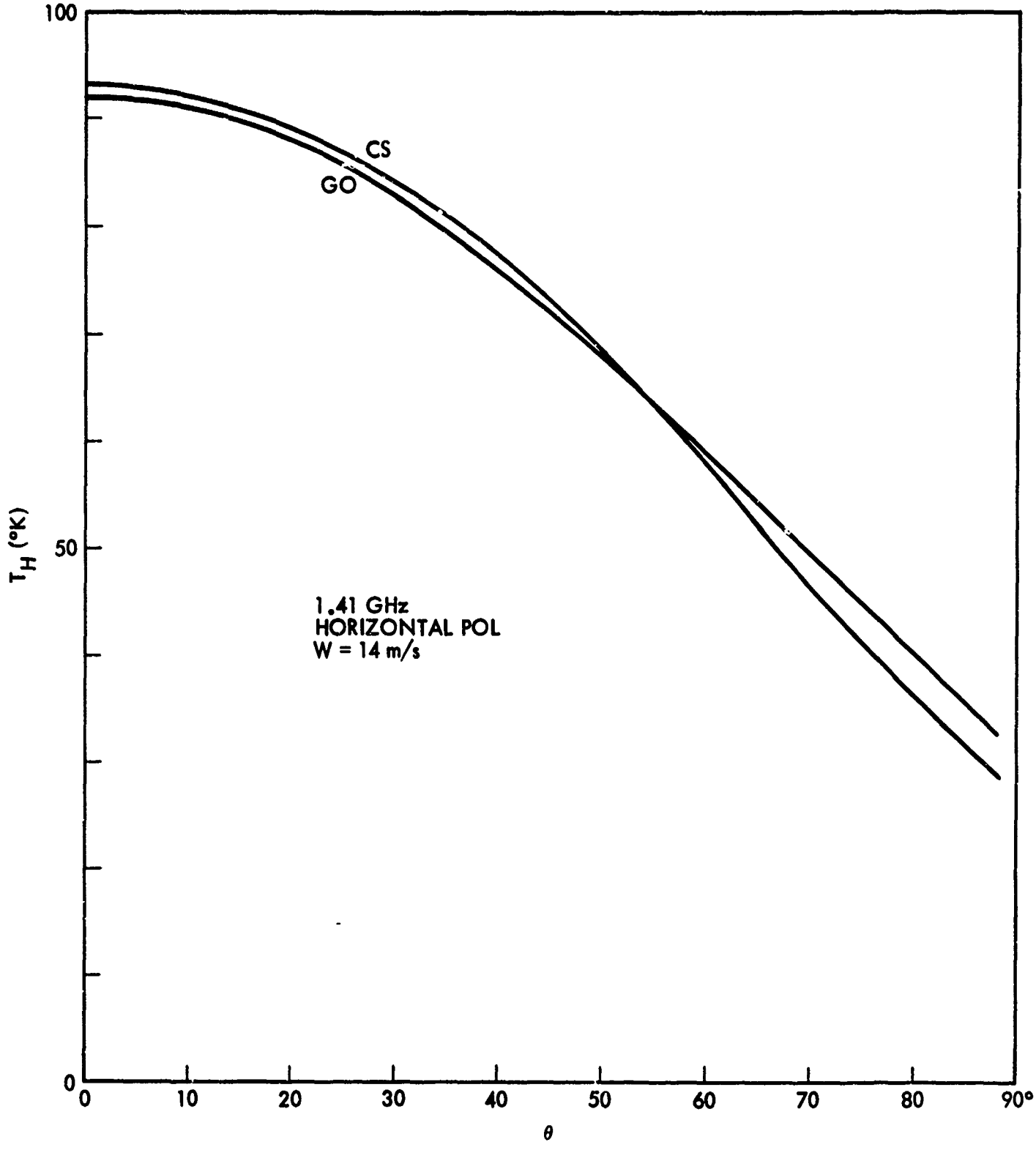

Fig. 21. Comparison of composite surface and geometrical optics brightness temperatures.

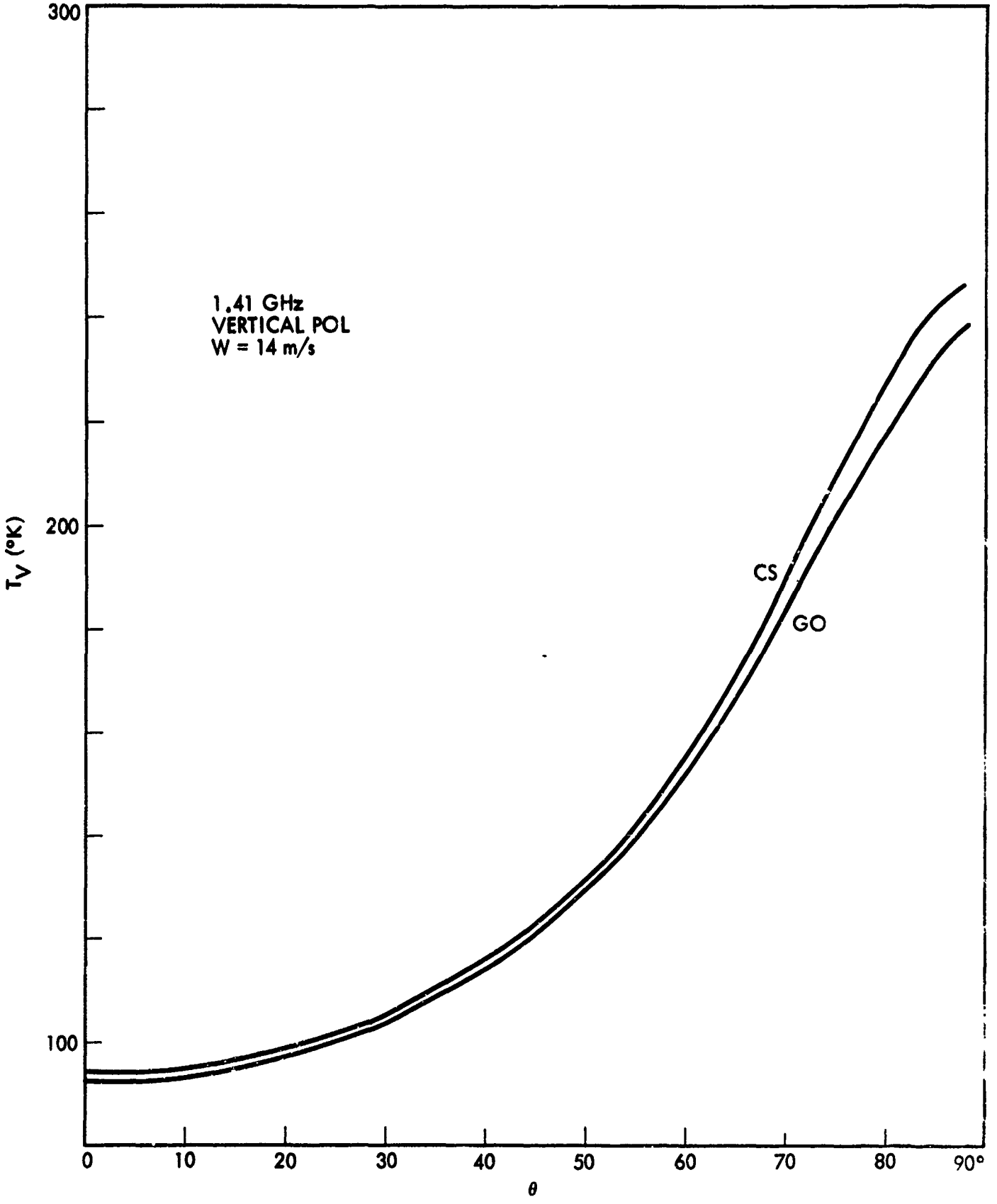

Fig. 22. Comparison of composite surface and geometrical optics brightness temperatures.

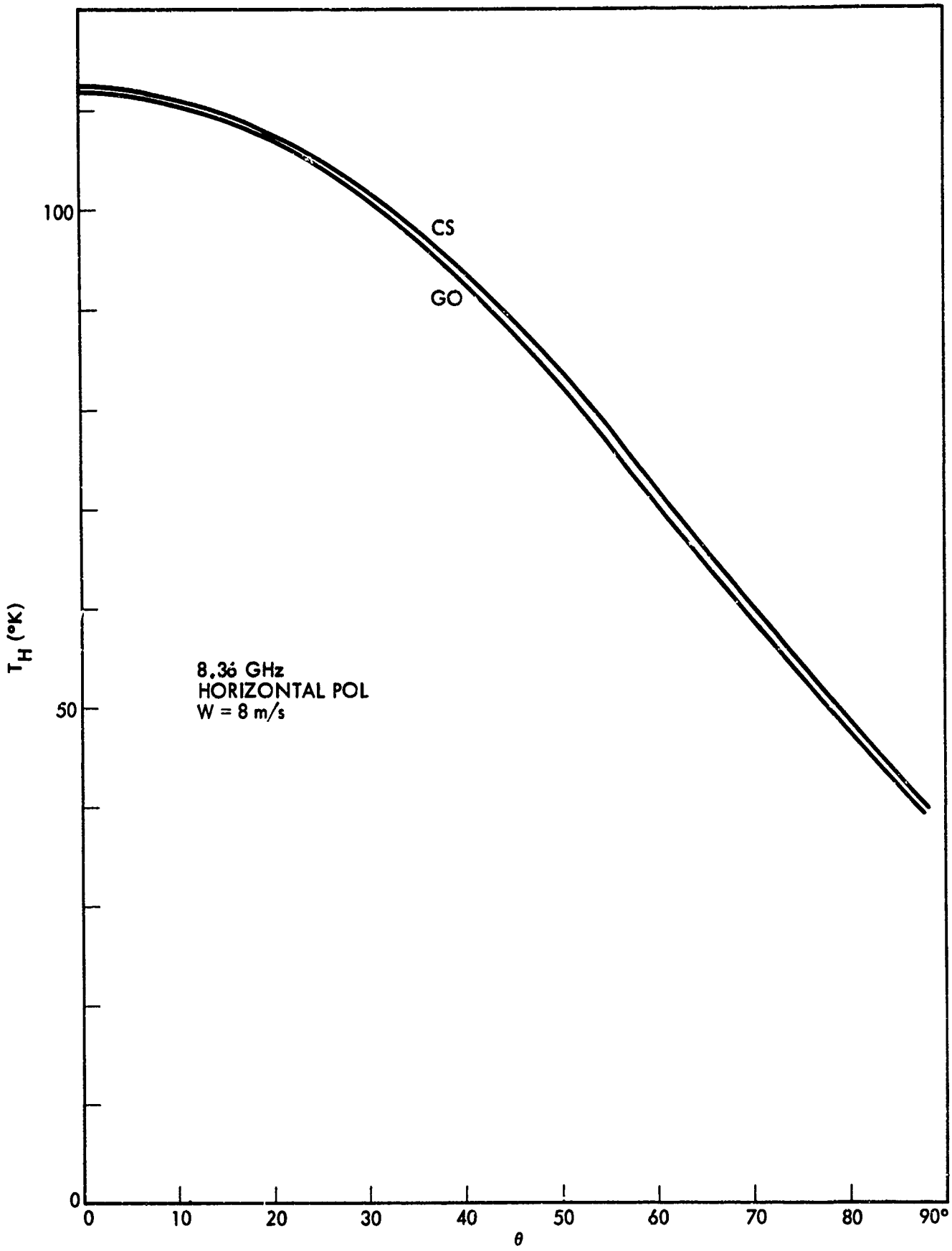

Fig. 23. Comparison of composite surface and geometrical optics brightness temperatures.

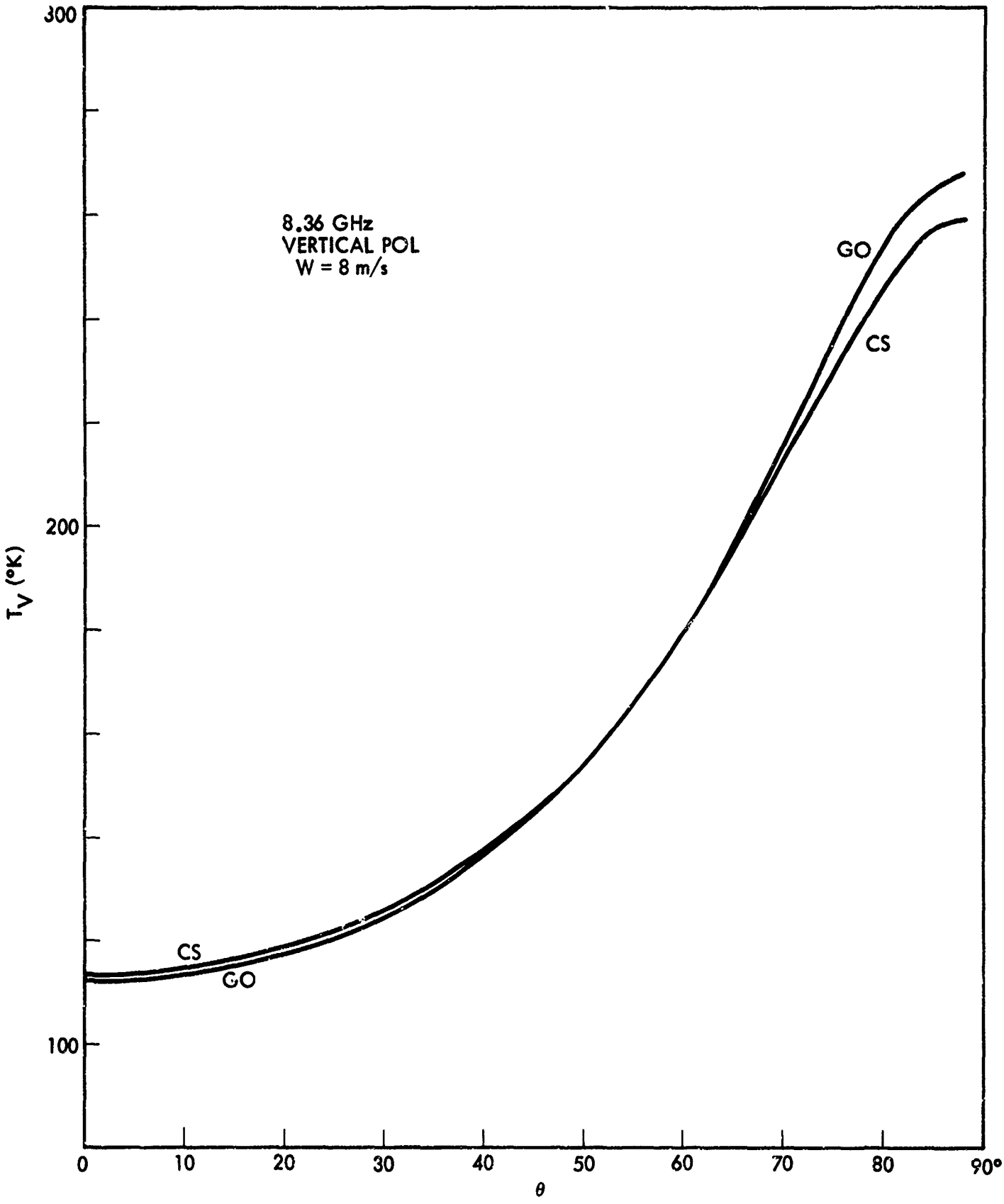

Fig. 24. Comparison of composite surface and geometrical optics brightness temperatures.

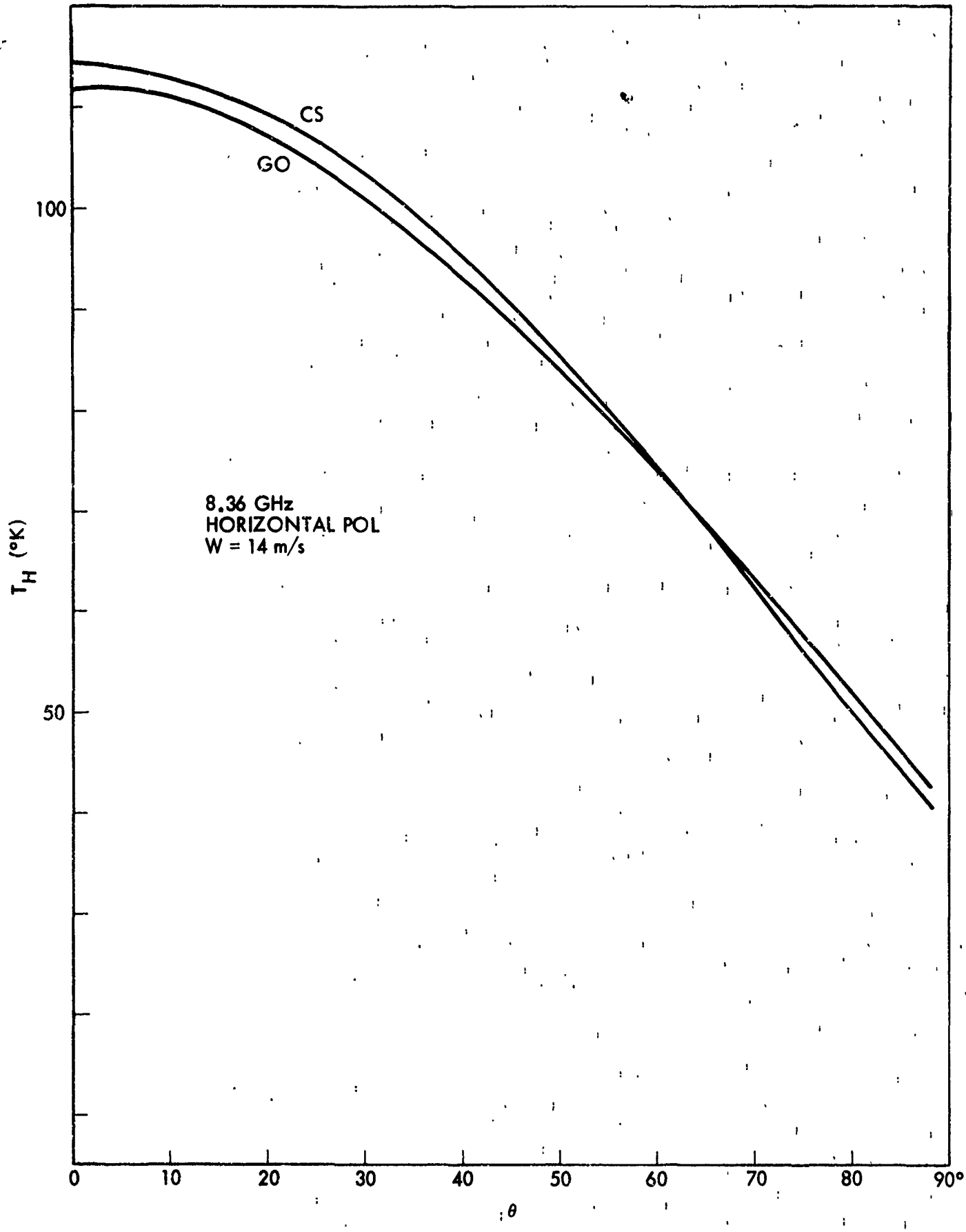

Fig. 25. Comparison of composite surface and geometrical optics brightness temperatures.

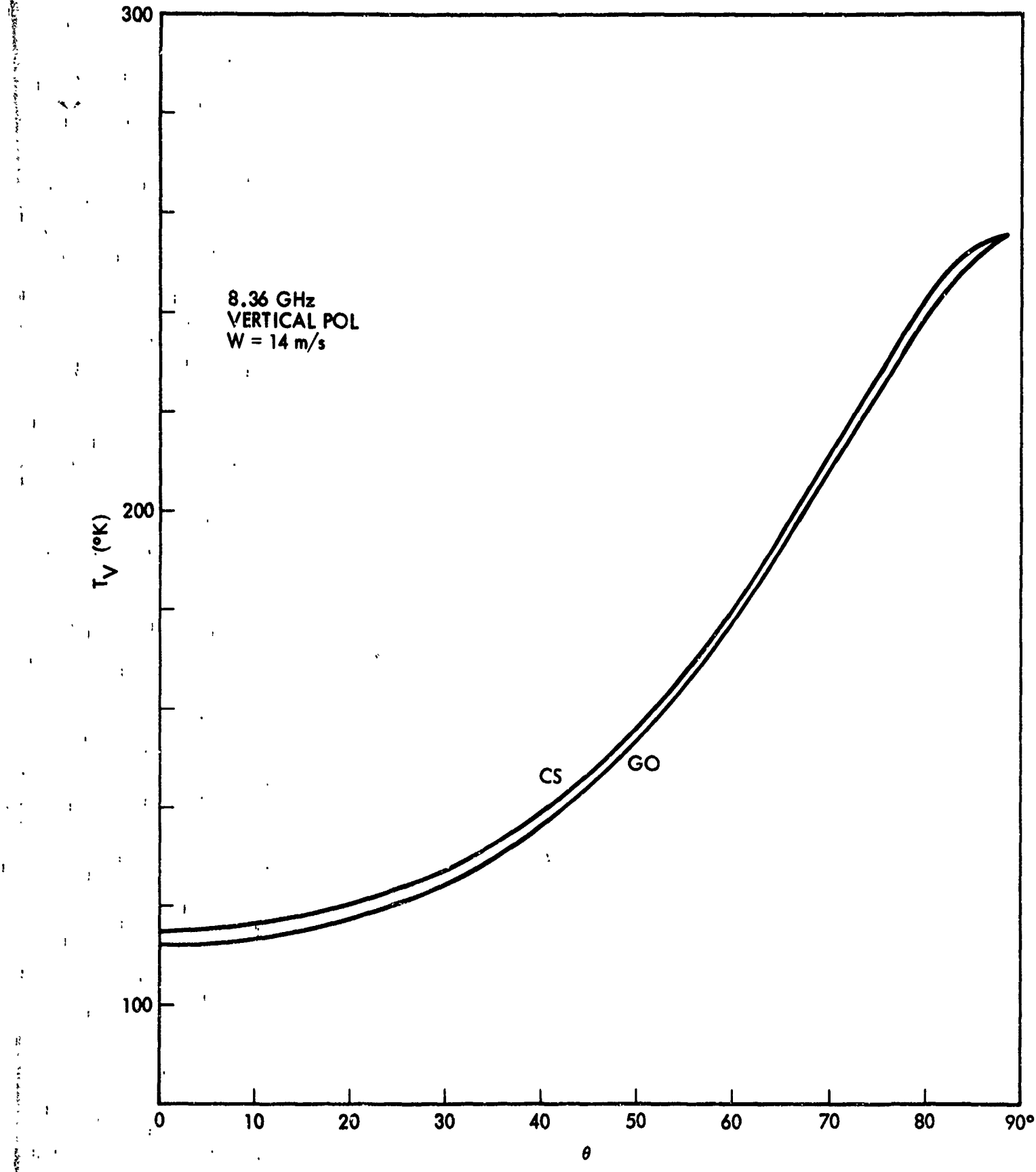

Fig. 26. Comparison of composite surface and geometrical optics brightness temperatures.

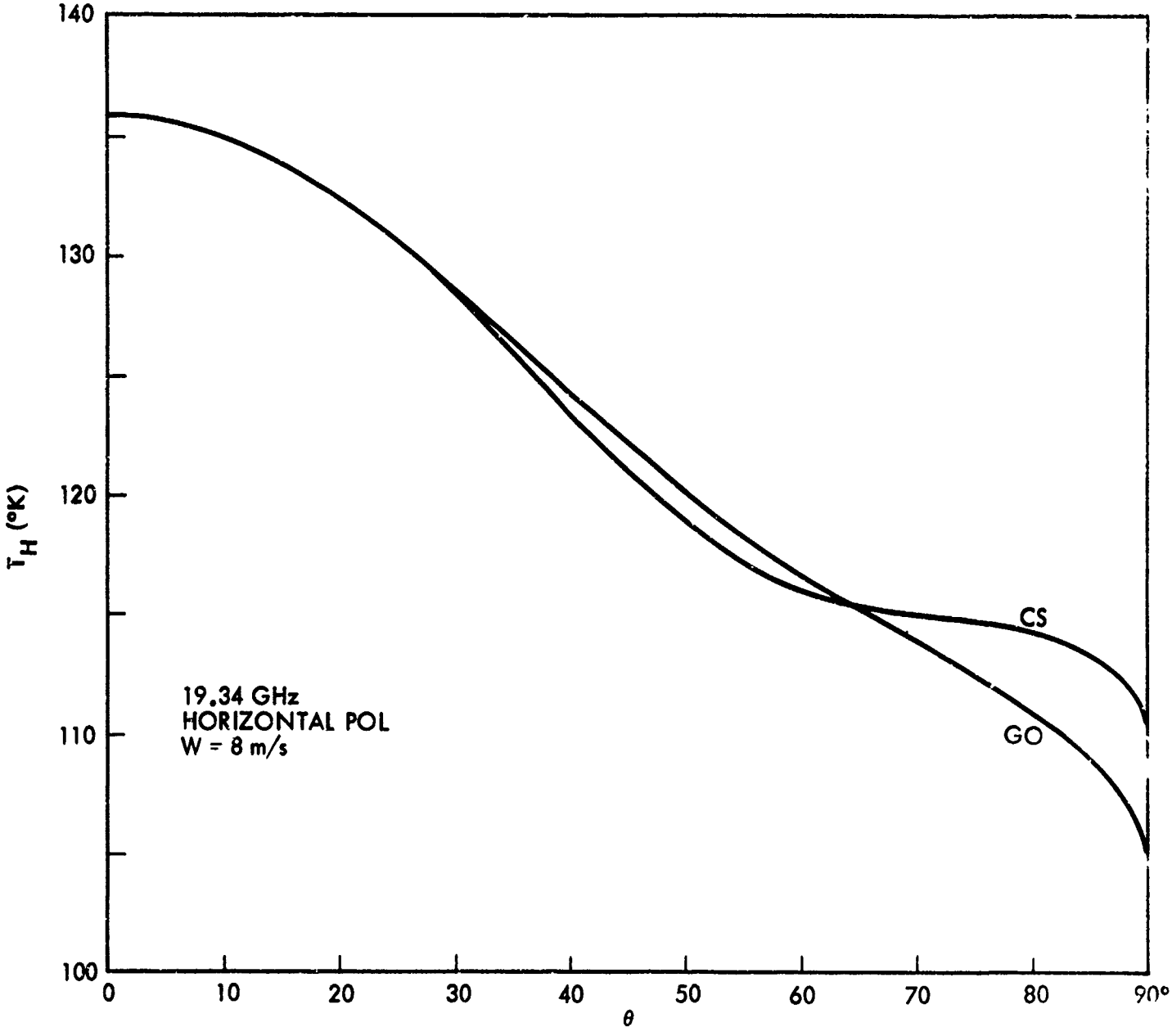

Fig. 27. Comparison of composite surface and geometrical optics brightness temperatures.

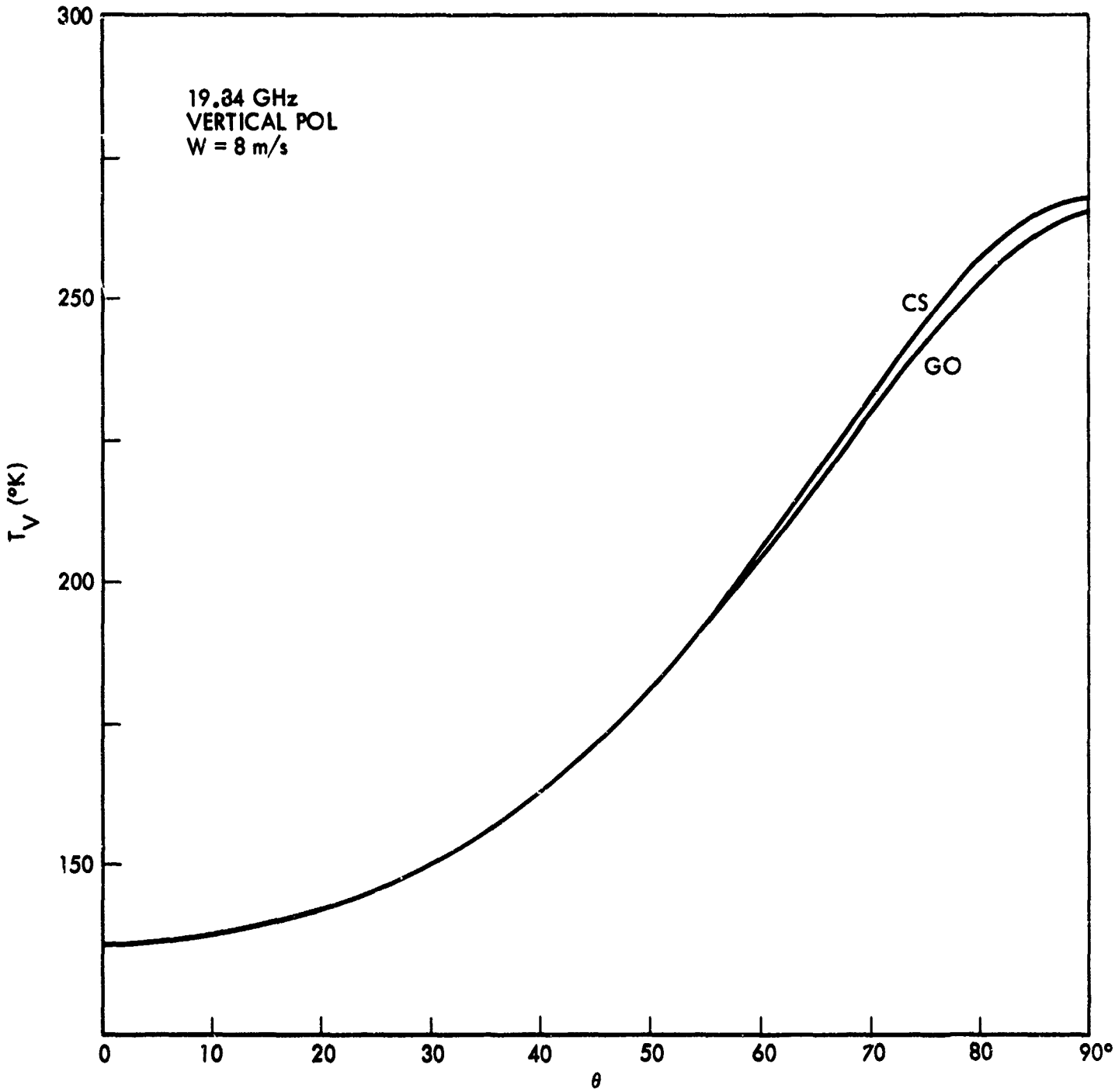

Fig. 28. Comparison of composite surface and geometrical optics brightness temperatures.

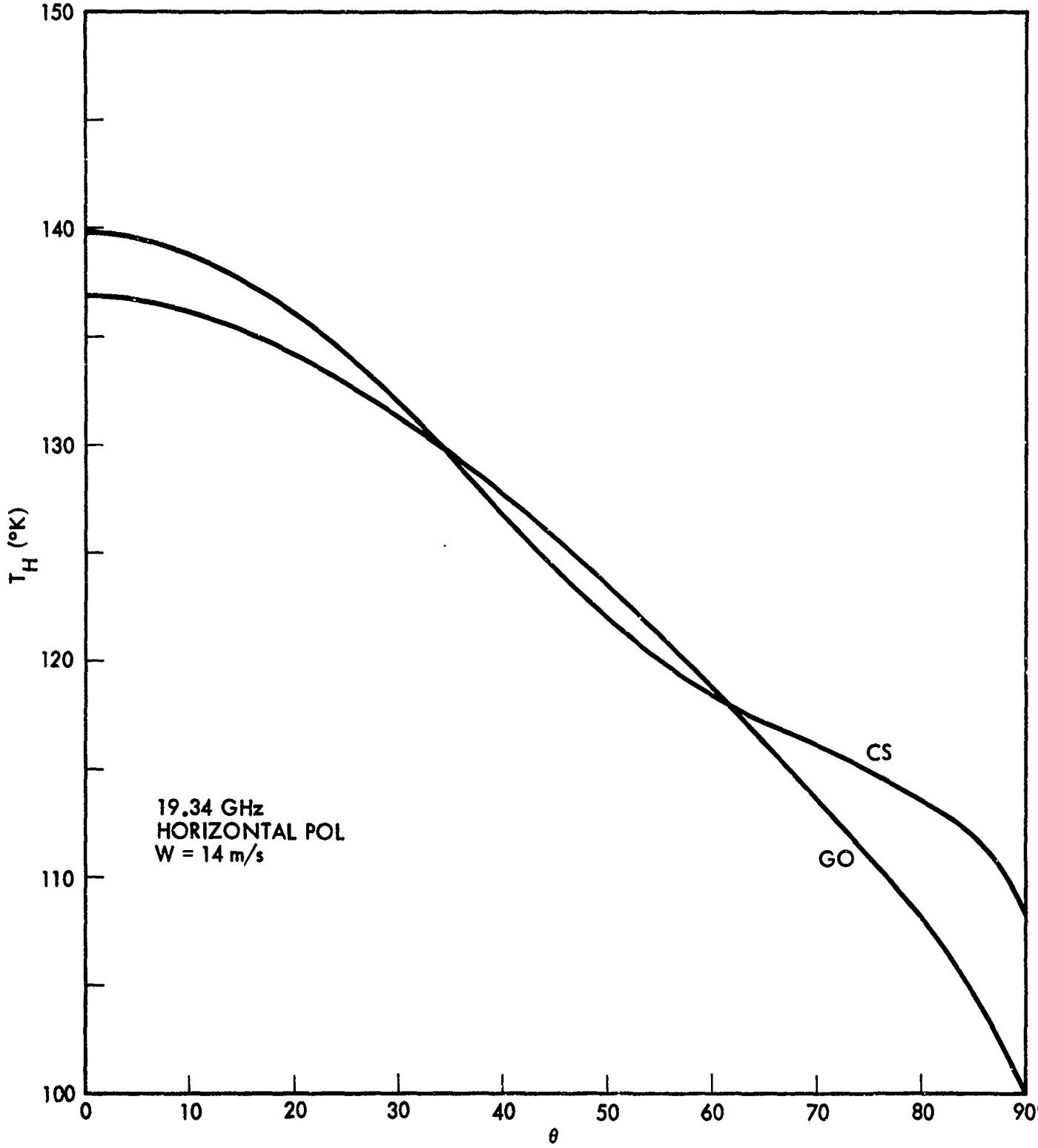

Fig. 29. Comparison of composite surface and geometrical optics brightness temperatures.

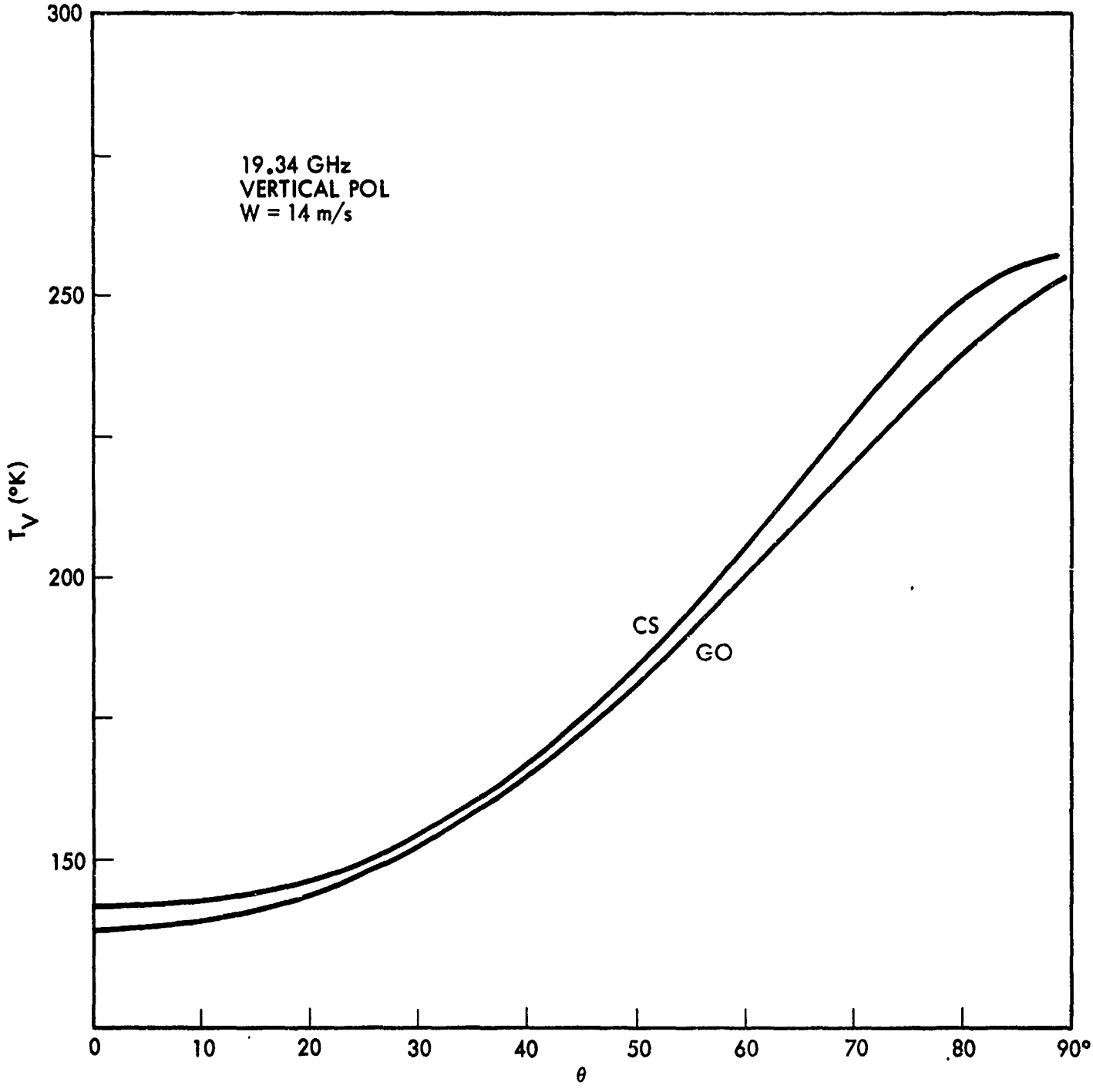

Fig. 30. Comparison of composite surface and geometrical optics brightness temperatures.

Figure 31 shows the wind speed dependence of the horizontally polarized sea brightness temperature at a frequency of 19.34 gHz and an observation angle of 55°; ΔT in this figure is defined to be the difference between the brightness temperature at wind speed W and that at zero wind speed. The solid curve is that calculated with the present theory, while the experimental points were reported by Hollinger.[8] The error bars on the right of figure represent the expected uncertainty in the data, as quoted by Hollinger. Experiment and theory appear to agree, within the experimental error.

In Fig. 32 is shown the change in the percentage polarization, P, with wind speed, where $P \equiv 100 \times (T_V - T_H)/(T_V + T_H)$. The solid line represents the theoretical values while the dashed line represents Hollinger's linear fit to his data. The two appear to be in agreement over the range of measured values. However, if the percentage polarization P, rather than ΔP, is compared with experiment, a constant difference of several percentage points is revealed, even for zero wind speed. Although a slight swell may remain at zero wind speed, a simple flat surface calculation — independent of any theory or model of surface roughness effects — should nevertheless correspond quite closely to the measurements. This is not the case and the reason for the discrepancy is not known, although a slight polarization mixing in the antenna might be suspected.

In Figure 33 we show the wind speed dependence of the vertically polarized brightness temperatures at a fixed observation angle of 55° and for the three frequencies of 1.41, 8.36, and 19.34 gHz. For the corresponding measurements of Hollinger, which are not shown in the figure, we refer the reader to reference 8. Hollinger fit his data with straight lines and quoted values of

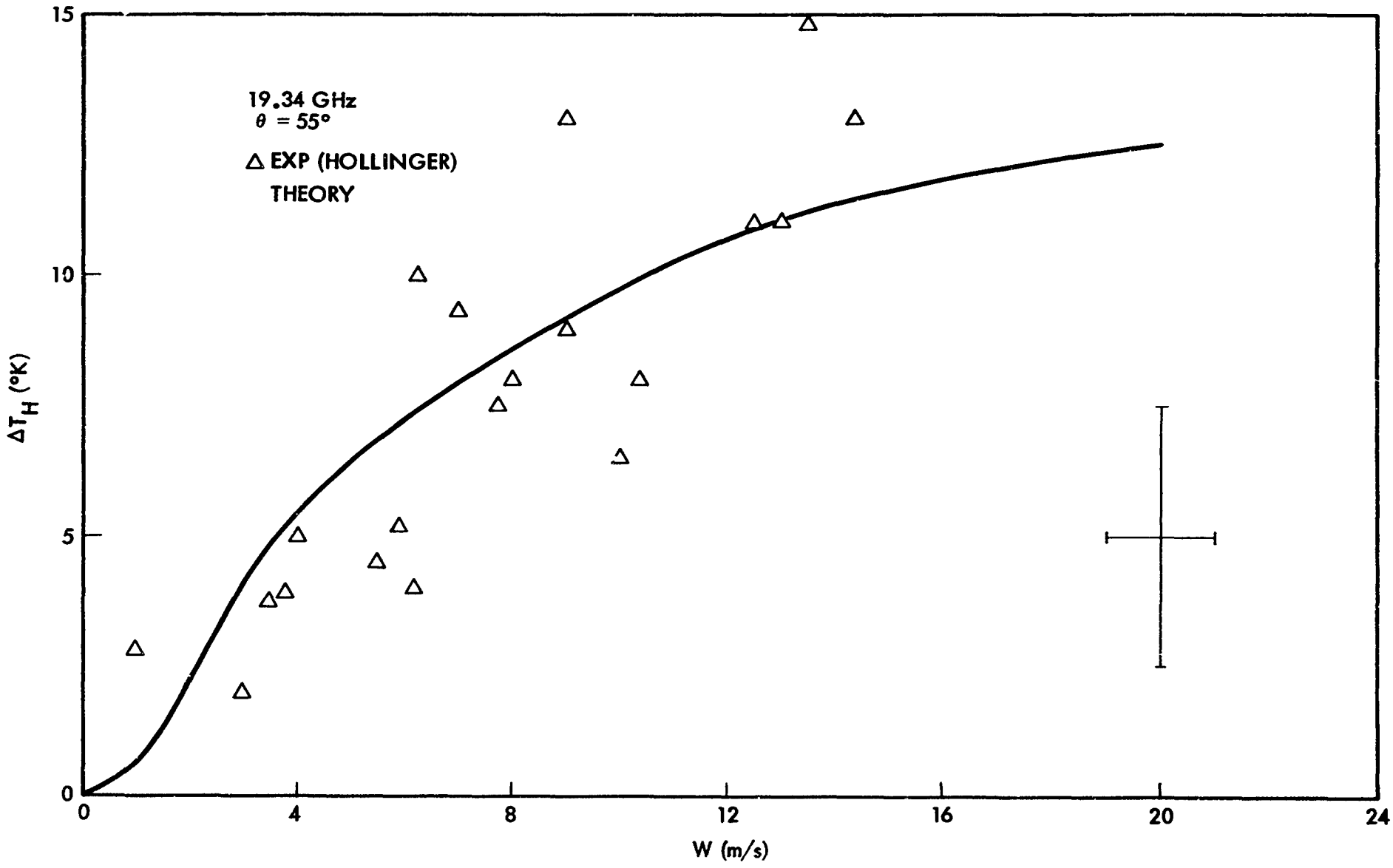

Fig. 31. Comparison of theoretical wind speed dependence at 19.34 gHz, $\theta = 55°$, with the experimental results of Hollinger. The error bars indicate the estimated measurement uncertainty.

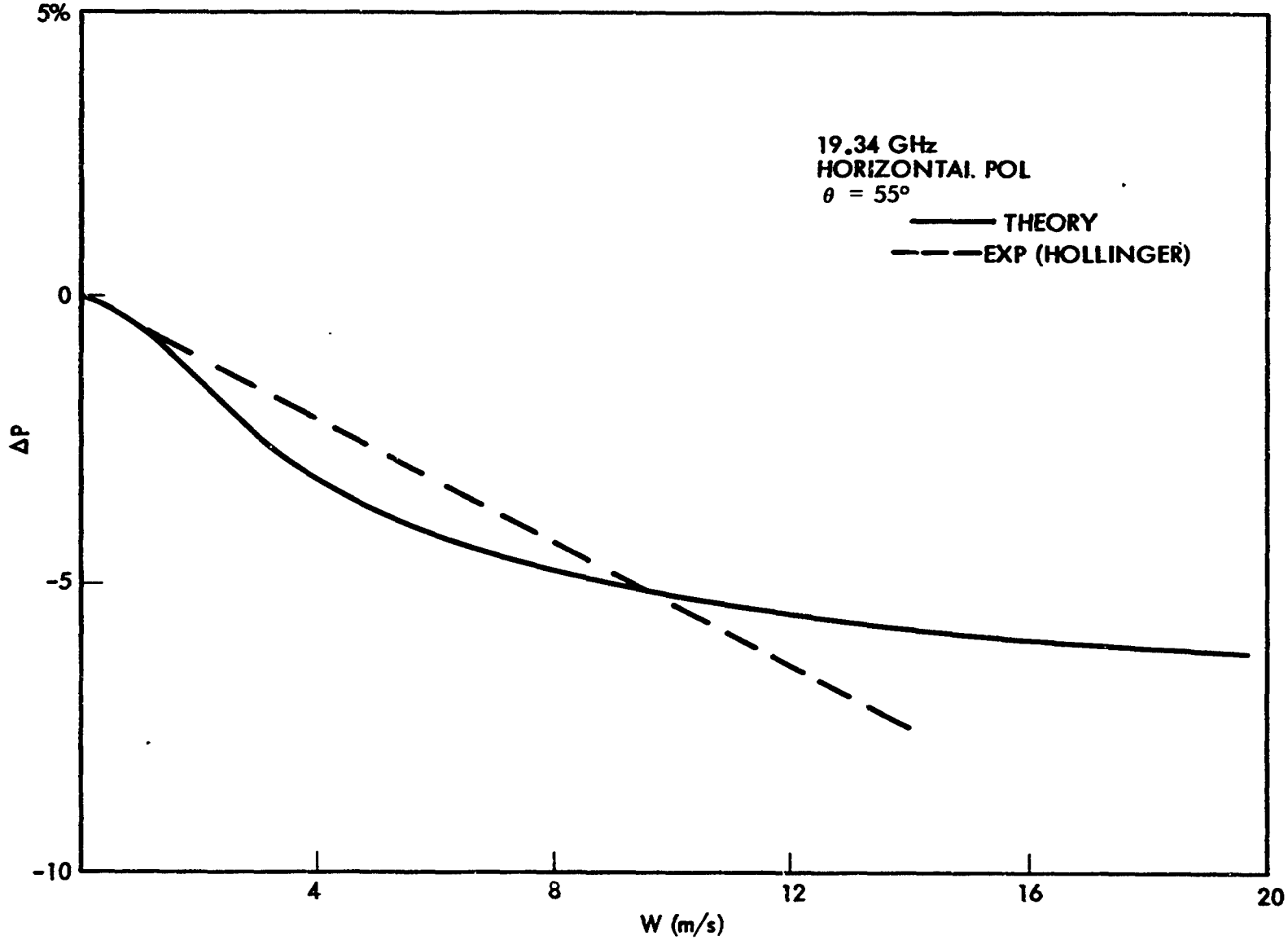

Fig. 32. Wind speed dependence of the percentage polarization at 19.34 gHz, θ = 55°. Comparison of theory with Hollinger's linear fit to the data.

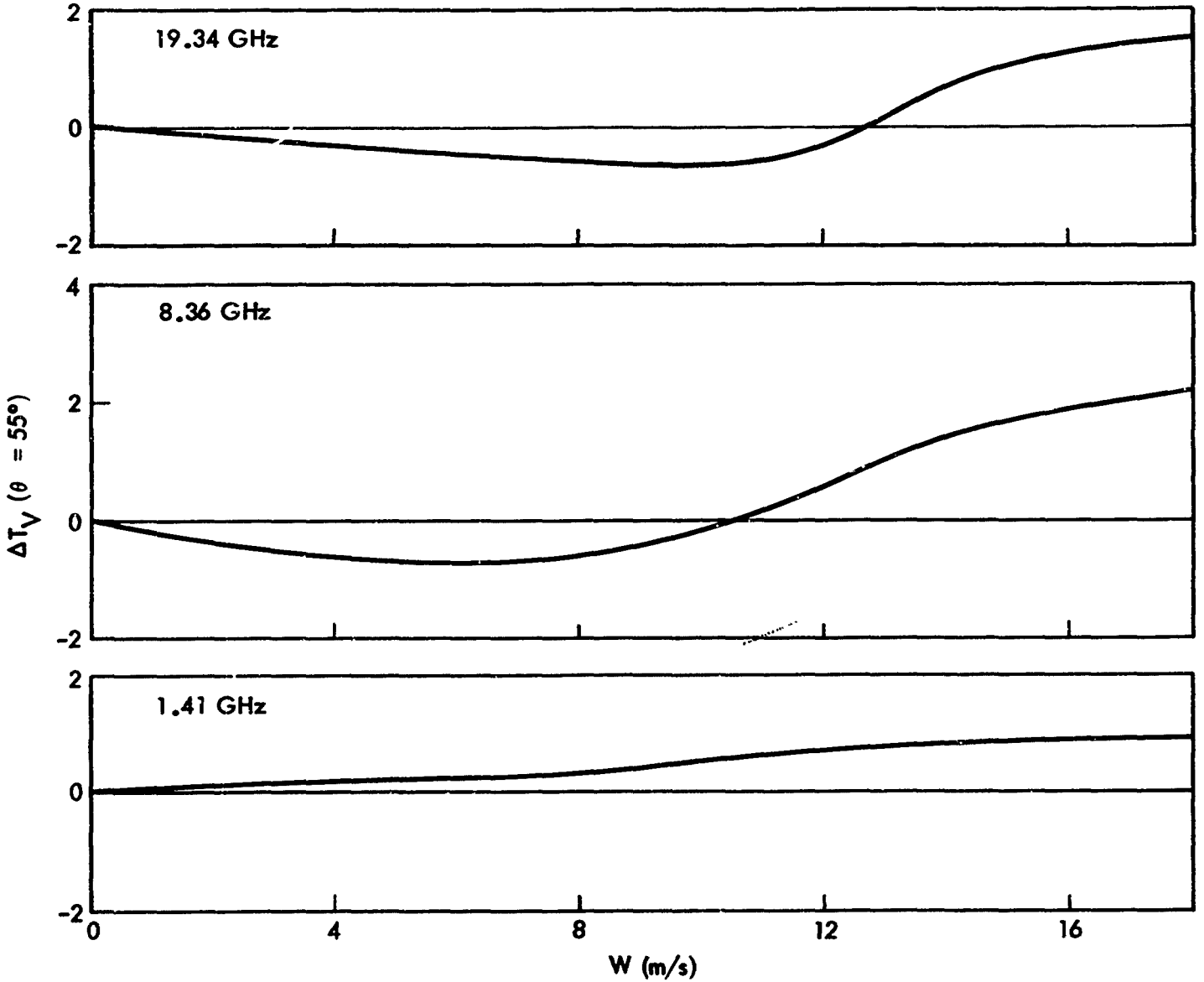

Fig. 33. Wind speed dependence of the vertically polarized sea brightness temperature at 3 frequencies and a fixed observation angle of 55°.

the slopes of the lines at the three frequencies. Because of the obviously nonlinear behavior of the theoretical curves it is difficult to assign a single value to $d(\Delta T)/dW$. However, examination of the data points and their expected uncertainty show the theoretical curves of Fig. 33 to lie well within the range of the measurements.

V. SUMMARY AND CONCLUSIONS

The second-order geometrical optics theory of emissivity and brightness temperature of a rough surface is extended to low frequencies by the introduction of a composite surface model in which the diffraction effects of surface roughness smaller than a wavelength are explicitly included. The total surface height spectrum is divided into a large-scale and a small-scale spectrum, with the separation point determined by the radiation frequency. The small-scale spectrum is assumed to describe the surface structure residing on a surface "element" of the large-scale structure. Equations for the emissivity of the small structure are derived using second-order perturbation theory. This roughness-dependent emissivity replaces the elemental smooth surface emissivity in the geometrical optics equations; the effect of the large-scale roughness is described by the same equations but with the roughness parameter now determined by only the large-scale spectrum. The composite surface model is shown to conserve energy to a high degree of approximation. The "direct emission" method of calculating rough surface emissivity is used to evaluate horizontally and vertically polarized sea bright brightness temperatures over a wide range of frequencies, wind speeds, water temperatures, salinities, and atmospheric conditions. The results are compared with those of the purely geometrical optics model and the differences are shown to be no more than a few degrees ($\lesssim 4°K$) except for very large observation angles. Significant differences ($\gtrsim 1°K$) do occur for all frequencies, both polarizations, and most wind speeds. Thus for applications which require calculations of this accuracy, use of the composite surface model is indicated. Theoretical and experimental sea brightness temperatures for both polarizations, three frequencies, and a range of wind speeds, are in good agreement.

APPENDIX — EMISSIVITY OF SLIGHTLY ROUGH SURFACES

In this Appendix we derive the equations for the emissivity of a rough surface whose height variations are small compared to the radiation wavelength. Expressions for the scattered electromagnetic field, defined as the difference between the total field and that due to a smooth plane, are used in a statement of energy conservation to yield an "optical theorem" for rough surface scattering. This equation expresses the emissivity as a sum of the flat-surface emissivity plus terms depending on roughness. Use of a Fourier integral representation for the scattered fields then provides an equation in which the emissivity is expressed directly in terms of the Fourier coefficients of the scattered fields. Perturbation solutions for the Fourier coefficients, known through second order in the perturbation parameter, are inserted into the emissivity equation, and averaging over an ensemble of surfaces having random surface height variations then leads to the desired equation in which the emissivity is given explicitly in terms of the two-dimensional surface height spectrum of the surface.

I. Asymptotic Limit of the Field

We consider a plane wave incident on the rough-surface boundary, $z = \zeta(x,y)$, which separates the source medium from a dielectric with index of refraction n (Fig. 34). The electric field satisfies the vector Helmholtz equation

$$\underset{\sim}{\nabla} \times \underset{\sim}{\nabla} \times \underset{\sim}{E} - k^2 \underset{\sim}{E} = 0 \qquad (1.1)$$

everywhere above the surface. We first consider the case of horizontal polarization. Then, if the direction of incidence is chosen to be in the x-z plane, the following Fourier representation for the electric field applies:

$$\underset{\sim}{E}^h(\underset{\sim}{r}) = \hat{y}[\exp(i\underset{\sim}{k}_o \cdot \underset{\sim}{r}) + R_h(\cos\theta_o)\exp(i\underset{\sim}{k}_o' \cdot \underset{\sim}{r})] + \underset{\sim}{E}^h_{sc}(\underset{\sim}{r}) \quad , \qquad (1.2)$$

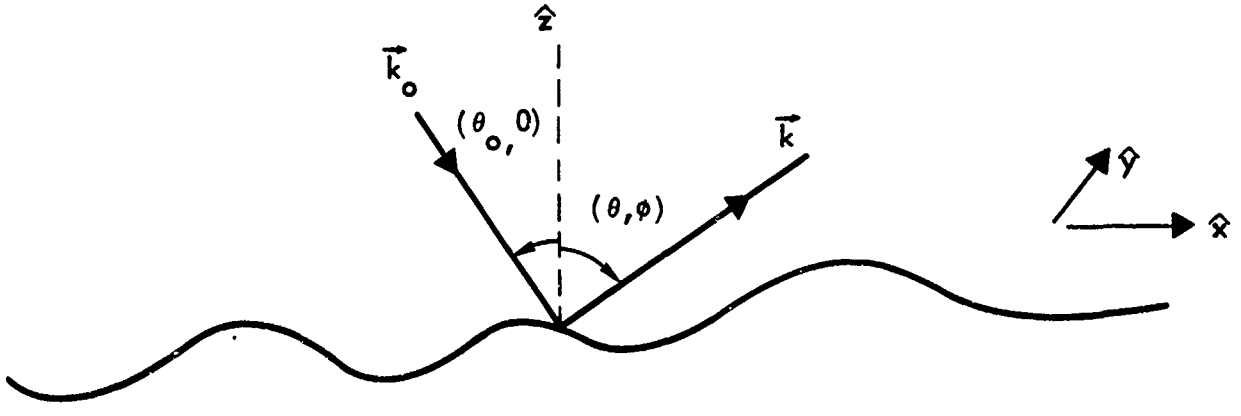

Fig. 34. Rough surface scattering geometry.

where

$$\underset{\sim}{E}^h_{sc} = \int_{-\infty}^{\infty} dK_x \int_{-\infty}^{\infty} dK_y \, \underset{\sim}{A}^h(K_x,K_y)\exp[i(K_x x + K_y y + b_K z)] \quad , \tag{1.3}$$

with

$$b_K = (k^2 - K_x^2 - K_y^2)^{\frac{1}{2}} \quad , \quad (K_x^2+K_y^2)^{\frac{1}{2}} < k$$

$$b_K = i(K_x^2+K_y^2-k^2)^{\frac{1}{2}} \quad , \quad (K_x^2+K_y^2)^{\frac{1}{2}} > k \quad , \tag{1.4}$$

and

$$\underset{\sim}{k}_o = k(-\sin\theta_o \, \hat{x} - \cos\theta_o \, \hat{z}) \quad ,$$

$$\underset{\sim}{k}'_o = k(-\sin\theta_o \, \hat{x} + \cos\theta_o \, \hat{z}) \quad . \tag{1.5}$$

The first term in the expression for the field is the flat-plane scattering result with reflection coefficient R_h. A perturbation expansion for the Fourier coefficients, valid when both the surface slope and the ratio of surface height to wavelength are small, was derived by Rice,[15] and the first few terms may be found in Sec. III of this Appendix.

The asymptotic form of Eq. (1.2) determines the scattering coefficient. We first introduce polar coordinates in Eq. (1.3) and then write

$$\underset{\sim}{E}^h_{sc} = \underset{\sim}{J}^h_1 + \underset{\sim}{J}^h_2 \quad , \tag{1.6}$$

where

$$\underset{\sim}{J}^h_1 = \int_o^k dK \, K \int_o^{2\pi} d\omega \, \underset{\sim}{A}^h(K\cos\omega, K\sin\omega)[\exp iK(x\cos\omega + y\sin\omega)] \, x$$
$$x[\exp i(k^2-K^2)^{\frac{1}{2}} z] \quad , \tag{1.7}$$

$$\underset{\sim}{J}^h_2 = \int_k^{\infty} dK \, K \int_o^{\pi} d\omega \, \underset{\sim}{A}^h(K\cos\omega, K\sin\omega)[\exp iK(x\cos\omega + y\sin\omega)] \, x$$
$$x \exp[-(K^2-k^2)^{\frac{1}{2}} z] \quad . \tag{1.8}$$

We change integration variables in Eq. (1.7) via the transformation $K = k\sin\gamma$ and, also, we introduce spherical coordinates (r,θ,ϕ) for (x,y,z):

$$\underset{\sim}{J}_1^h = k^2 \int_0^{2\pi} d\omega \int_0^{\pi/2} d\gamma \, \sin\gamma \cos\gamma \, \underset{\sim}{A}^h(k\sin\gamma\cos\omega, k\sin\gamma\sin\omega) \exp[ikr(\hat{k}\cdot\hat{r})] \, , \tag{1.9}$$

where

$$\hat{k}\cdot\hat{r} = \cos\gamma\cos\theta + \sin\gamma\sin\theta\cos(\omega-\phi) \, . \tag{1.10}$$

The following relation[17] between plane wave and spherical waves holds in the asymptotic limit:

$$\exp[ikr(\hat{k}\cdot\hat{r})] \xrightarrow[r\to\infty]{} \left(\frac{1}{ikr}\right) [\delta(1-\hat{k}\cdot\hat{r}) \exp(ikr) - \delta(1+\hat{k}\cdot\hat{r})\exp(-ikr)] \, . \tag{1.11}$$

By substitution of Eq. (1.11) into Eq. (1.9), we then obtain

$$\underset{\sim}{J}_1^h \xrightarrow[r\to\infty]{} \left(\frac{2\pi k}{i}\right) (\cos\theta) \, \underset{\sim}{A}^h(k\sin\theta\cos\phi, k\sin\theta\sin\phi) \, \frac{[\exp ikr]}{r} \, , \tag{1.12}$$

for the delta function which multiplies the incoming spherical wave is always zero for the integration range $0 < \gamma < \pi/2$.

The remaining quantity, $\underset{\sim}{J}_2^h$, contains a dying exponential factor. Because of this exponential factor, the magnitude of $\underset{\sim}{J}_2^h$ can be shown to drop off at least as rapidly as z^{-2}, when z is more than a few wavelengths above the medium plane. The dominant term in the asymptotic region is therefore $\underset{\sim}{J}_1^h$. Thus, from Eqs. (1.2), (1.6), and (1.12), we have

$$\underset{\sim}{E}^h(\underset{\sim}{r}) \xrightarrow[r\to\infty]{} \hat{y}[\exp(i\underset{\sim}{k}_o\cdot\underset{\sim}{r}) + R_h \exp(i\underset{\sim}{k}_o'\cdot r)] + \underset{\sim}{F}^h(\underset{\sim}{k},\underset{\sim}{k}_o)\frac{[\exp(ikr)]}{r} \, , \tag{1.13}$$

where

$$\underset{\sim}{F}^h(\underset{\sim}{k},\underset{\sim}{k}_o) = \left(\frac{2\pi k}{i}\right)(\cos\theta) \, \underset{\sim}{A}^h(k\sin\theta\cos\phi, \, k\sin\theta\sin\phi) \, . \tag{1.14}$$

Similar results apply for vertically polarized incident radiation. We will describe the vertical polarization state by the magnetic field. Then, the equations analogous to Eqs. (1.2), (1.13), and (1.14) are

$$\underset{\sim}{H}^{v}(\underset{\sim}{r}) = \hat{y}[\exp(i\underset{\sim}{k}_{o}\cdot\underset{\sim}{r}) + R_{v}(\cos\theta_{o})\exp(i\underset{\sim}{k}_{o}\cdot\underset{\sim}{r})] + \int_{-\infty}^{\infty} dK_{x} \int_{-\infty}^{\infty} dK_{y}\, \underset{\sim}{A}^{v}(K_{x},K_{y})\exp[i(K_{x}x + K_{y}y + b_{K}z)] \quad , \tag{1.15}$$

$$\underset{\sim}{H}^{v}(\underset{\sim}{r}) \xrightarrow[r\to\infty]{} \hat{y}[\exp(i\underset{\sim}{k}_{o}\cdot\underset{\sim}{r}) + R_{v}(\cos\theta_{o})\exp(i\underset{\sim}{k}'_{o}\cdot\underset{\sim}{r})] + \underset{\sim}{F}_{v}(\underset{\sim}{k},\underset{\sim}{k}_{o})\frac{[\exp(ikr)]}{r} \quad , \tag{1.16}$$

$$\underset{\sim}{F}^{v}(k,k_{o}) = \left(\frac{2\pi k}{i}\right)(\cos\theta)\ \underset{\sim}{A}^{v}(k\sin\theta\cos\phi,\ k\sin\theta\sin\phi) \quad . \tag{1.17}$$

II. Optical Theorem

We first take the scalar product of Eq. (1.1) with $\underset{\sim}{E}^{*}$, then subtract the complex conjugate of this operation and, finally, integrate the result over the region bounded by the rough surface and a hemisphere of very large radius. The application of the divergence theorem yields the surface integral

$$\int_{T} d\underset{\sim}{S}\cdot\underset{\sim}{N} = 0 \quad , \tag{2.1}$$

where

$$\underset{\sim}{N} = \frac{1}{2}\,\mathrm{Re}(\underset{\sim}{E}\times\underset{\sim}{H}^{*}) \quad . \tag{2.2}$$

Equation (2.1) may be rewritten as

$$\int_{S} d\underset{\sim}{S}\cdot\underset{\sim}{N} = \int_{\rho} d\underset{\sim}{S}\cdot\underset{\sim}{N} \quad , \tag{2.3}$$

where S represents the hemisphere, ρ is the rough surface, and T is the total surface. Equation (2.1) is a statement of energy conservation; i.e., absorption and scattering by the rough surface must balance the incident energy flow. This means that the left-hand side of Eq. (2.3) must be proportional to the incident power minus the total scattered outflow. Indeed, the substitution of the usual asymptotic form of the scattering solution,

$$\underset{\sim}{E}^h(\underset{\sim}{r}) \underset{r\to\infty}{\longrightarrow} \hat{y}\exp(i\underset{\sim}{k}_o\cdot\underset{\sim}{r}) + \underset{\sim}{f}^h(\underset{\sim}{k},\underset{\sim}{k}_o)\frac{[\exp(ikr)]}{r} \quad , \tag{2.4}$$

into this integral yields

$$I \equiv \int_S d\underset{\sim}{S}\cdot\underset{\sim}{N}^h \tag{2.5}$$

$$= \frac{-S_o}{2\mu_o c}\left[1 - \int_U d\Omega\gamma^h(\underset{\sim}{k},\underset{\sim}{k}_o)\right] \tag{2.6}$$

$$I = \frac{-S_o}{2\mu_o c}\, e^h(-\underset{\sim}{k}_o) \quad . \tag{2.7}$$

The quantity γ is the scattering coefficient; it is defined as

$$S_o\,\gamma^h(\underset{\sim}{k},\underset{\sim}{k}_o) \equiv |\underset{\sim}{f}^h(\underset{\sim}{k},\underset{\sim}{k}_o)|^2 \quad . \tag{2.8}$$

Here, the power incident on the segment of rough surface subtended by the hemisphere S (of radius r) is unit intensity times S_o, the projection of the surface area in the direction of incidence:

$$S_o = \pi r^2 \cos\theta_o \quad . \tag{2.9}$$

Finally, $e^h(-\underset{\sim}{k}_o)$ is the horizontally polarized emissivity of the rough surface, with Eq. (2.7) following from Eq. (2.6) via a theorem due to Peake.[2] Equation (2.7) can be written explicitly in terms of the fields by use of Eq. (2.2):

$$e^h(-\underset{\sim}{k}_o) = \frac{-\mu_o c}{S_o} \operatorname{Re} \int_S d\underset{\sim}{S} \cdot (\underset{\sim}{E}^h \times \underset{\sim}{H}^{h^*}) \quad . \tag{2.10}$$

We now proceed to the derivation of the optical theorem by the substitution of the asymptotic representation Eq. (1.13) into Eq. (2.10). This approach insures a nonzero interference term. The asymptotic magnetic field, $\underset{\sim}{H}^h$, is determined from $\underset{\sim}{E}^h$ via Maxwell's equations:

$$\mu_o c \, \underset{\sim}{H}^h \xrightarrow[r \to \infty]{} (\hat{k}_o \times \hat{y}) \exp(i\underset{\sim}{k}_o \cdot \underset{\sim}{r}) + (\hat{k}'_o \times \hat{y}) \, R_h \exp(i\underset{\sim}{k}_o \cdot \underset{\sim}{r})$$

$$+ [\hat{r} \times \underset{\sim}{F}^h(\underset{\sim}{k}, \underset{\sim}{k}_o)] \frac{[\exp(ikr)]}{r} \quad . \tag{2.11}$$

Three sets of terms then arise from the cross multiplication in Eq. (2.10). The first set, involving products of plane-wave terms only, must lead to the flat-plane emissivity as roughness effects are contained only in $\underset{\sim}{F}^h$. The second set of terms describes interference between the specularly scattered plane wave and the outgoing spherical wave, with the result that the scattering coefficient is evaluated in the specular direction. The third set contains the single term representing the scattered intensity. After some algebra and frequent application of Eq. (1.11), we arrive at the following result:

$$e^h(-\underset{\sim}{k}_o) \quad 1 - |R_h(\cos\theta_o)|^2 + \left|\frac{4\pi}{kS_o}\right| \mathcal{J}m\{R_h^*(\cos\theta_o)[\hat{y} \cdot \underset{\sim}{F}^h(\underset{\sim}{k}'_o, \underset{\sim}{k}_o)]\}$$

$$- \frac{1}{S_o} \int_U d\Omega |\underset{\sim}{F}^h(k\hat{r}, \underset{\sim}{k}_o)|^2 \quad . \tag{2.12}$$

The angular integration is over the upper hemisphere.

The first term in Eq. (2.12) is the emissivity of a plane surface. The remaining two terms describe the effects of surface roughness. A check on this result follows from consideration of a perfectly conducting surface. Then, by

Kirchhoff's law, the emissivity must vanish because the absorptivity is zero. Since $R_h = -1$ for a perfect conductor, Eq. (2.12) reduces to

$$\frac{-4\pi}{k} \mathrm{Im}[\hat{y}\cdot\underset{\sim}{F}^h(\underset{\sim}{k}'_o,\underset{\sim}{k}_o)] = \int_U d\Omega |\underset{\sim}{F}^h(k\hat{r},\underset{\sim}{k}_o)|^2 \quad . \tag{2.13}$$

This is the expected optical theorem for a conductor; the minus sign in Eq.(2.13) arises because it is the reflected plane wave which interferes with the spherical wave.

Finally, we relate the emissivity to the Fourier transform of Sec. I by substitution of Eq. (1.14) into Eq. (2.12). Because of the choice of the magnetic field to describe vertical polarization, Eq. (1.15), the same formal relation between emissivity and Fourier transform holds for both polarizations:

$$e^i(-\underset{\sim}{k}_o) = [1-|R_i(\cos\theta_o)|^2] - \frac{8\pi^2}{S_o}(\cos\theta_o)\mathrm{Re}\{R_i^*[\hat{y}\cdot\underset{\sim}{A}^i(k_{ox},0)]\}$$

$$- \frac{(2\pi k)^2}{S_o}\int_U d\Omega \cos^2\theta |\underset{\sim}{A}^i(k\sin\theta\cos\phi,\ k\sin\theta\sin\phi)|^2,$$

$$i = h,v \tag{2.14}$$

Rough-surface corrections to the emissivity can now be determined from approximate expressions for the Fourier transform.

III. Ensemble Averages

We can write the vector transform in terms of components:

$$\underset{\sim}{A}^i(K_x,K_y) = \alpha^i(K_x,K_y)\,\hat{x} + \beta^i(K_x,K_y)\,\hat{y} + \gamma^i(K_x,K_y)\,\hat{z}\ , \quad i = h,v. \tag{3.1}$$

In the procedure due to Rice, each component is expanded as, say,

$$\alpha^i(K_x,K_y) = \alpha_1^i(K_x,K_y) + \alpha_2^i(K_x,K_y) + \ldots\ , \quad i = h,v\ , \tag{3.2}$$

where α_1^i is first order in surface height, α_2^i is second order in surface height, etc. The α_j^i are determined by the requirement of continuity for the tangential electric and magnetic fields at the surface boundary. Explicit expressions for the analogous first- and second-order Fourier series coefficients were given by Valenzuela.[18] These expressions have been transformed here to reflect notational differences as well as our use of Fourier integral rather than Fourier series.

The results for horizontally polarized incident radiation will be considered first. The components $(\alpha^h, \beta^h, \gamma^h)$ correspond directly to the Valenzuela (A^h, B^h, C^h). If the spectrum of the surface profile is represented as

$$\zeta(x,y) = \int_{-\infty}^{\infty} dp \int_{-\infty}^{\infty} dq \; S(p,q) \exp[i(p_x x + q_y)], \tag{3.3}$$

with

$$S^*(p,q) = S(-p,-q) \quad , \tag{3.3a}$$

then the first-order coefficients are

$$\alpha_1^h(K_x,K_y) = \mu_1^h \, S(K_x - k_{ox}, K_y) \quad ,$$

$$\beta_1^h(K_x,K_y) = \mu_2^h \, S(K_x - k_{ox}, K_y) \quad ,$$

$$\gamma_1^h(K_x,K_y) = \mu_3^h \, S(K_x - k_{ox}, K_y) \quad , \tag{3.4}$$

where

$$\mu_1^h = \frac{-iV_h K_x K_y}{(c+bn^2)} \quad ,$$

$$\mu_2^h = \frac{iV_h(bc+K_x^2)}{(c+bn^2)} \quad ,$$

$$\mu_3^h = \frac{-iV_h CK_y}{(c+bn^2)} \quad , \tag{3.5}$$

and

$$V_h = (n^2-1)(1+R_h) \quad ,$$

$$b = (k^2-K_x^2-K_y^2)^{\frac{1}{2}} \quad ,$$

$$c = (k^2n^2-K_x^2-K_y^2)^{\frac{1}{2}} \quad . \tag{3.6}$$

Inspection of Eq. (2.14) shows that only $\beta_2(K_x,K_y)$ is required to provide an expression for emissivity valid thru second order in surface height. Indeed, we require β_2 evaluated at $K_x = k_{ox} = k\sin\theta_o$, $K_y = 0$:

$$\left[\cos\theta_o+(n^2-\sin^2\theta_o)^{\frac{1}{2}}\right]\beta_2^h(k_{ox},0) = \int_{-\infty}^{\infty} dK_x \int_{-\infty}^{\infty} dK_y \left[\nu_1^h+\nu_2^h(K_x,K_y)\right] S(k_{ox}-K_x,-K_y) \times S(K_x-k_{ox},K_y), \tag{3.7}$$

where

$$\nu_1^h = k^2V_h(n^2-\sin^2\theta_o)^{\frac{1}{2}}$$

$$\nu_2^h = -k(n^2-1)V_h\frac{(bc+K_x^2)}{(c+bn^2)} \quad . \tag{3.8}$$

The approach for vertically polarized incident radiation must be modified slightly because the coefficients (A^v,B^v,C^v) as given by Valenzuela are for the electric field while the coefficients $(\alpha^v,\beta^v,\gamma^v)$ of this paper are for the magnetic field. However, it is easy to show that the two sets of coefficients are related by

$$\begin{aligned}
\alpha^v(K_x,K_y) &= -(kb)^{-1}\left[K_xK_yA^v+(b^2+K_y^2)B^v\right] \quad , \\
\beta^v(K_x,K_y) &= k^{-1}(bA^v-K_xC^v) \quad , \\
\gamma^v(K_x,K_y) &= k^{-1}(K_xB^v-K_yA^v) \quad , \qquad (3.9)
\end{aligned}$$

where (A^v,B^v,C^v) are functions of (K_x,K_y). We can now write down the first-order coefficients of interest:

$$\begin{aligned}
\alpha_1^v(K_x,K_y) &= \mu_1^v\, S(K_x-k_{ox},K_y) \quad , \\
\beta_1^v(K_x,K_y) &= \mu_2^v\, S(K_x-k_{ox},K_y) \quad , \\
\gamma_1^v(K_x,K_y) &= \mu_3^v\, S(K_x-k_{ox},K_y) \quad , \qquad (3.10)
\end{aligned}$$

where

$$\begin{aligned}
\mu_1^v &= \frac{iV_vK_y}{(c+bn^2)}\left[-k_{ox}+\frac{K_x}{kn^2}(n^2-\sin^2\theta_o)^{\frac{1}{2}}(c-b)\right] \quad , \\
\mu_2^v &= \frac{-iV_v}{(c+bn^2)}\left\{-k_{ox}K_x+\frac{1}{kn^2}(n^2-\sin^2\theta_o)^{\frac{1}{2}}\left[c(k^2-K_y^2)+bK_y^2\right]\right\} \quad , \\
\mu_3^v &= \frac{iV_v(bc+K_x^2+K_y^2)}{(c+bn^2)}\left[\frac{K_y}{kn^2}(n^2-\sin^2\theta_o)^{\frac{1}{2}}\right] \quad , \qquad (3.11)
\end{aligned}$$

and

$$V_v = (n^2-1)(1+R_v) \quad . \qquad (3.12)$$

The second-order coefficient, $\beta_2^v(k_{ox},0)$, required for the emissivity calculation is

$$\left[n^2\cos\theta_o+(n^2-\sin^2\theta_o)^{\frac{1}{2}}\right]\beta_2^v(k_{ox},0) = \int_{-\infty}^{\infty}dK_x\int_{-\infty}^{\infty}dK_y\left[\nu_1^v+\nu_2^v(K_x,K_y)\right]\times$$

$$\times S(k_{ox}-K_x,-K_y)S(K_x-k_{ox},K_y) \quad , \qquad (3.13)$$

where

$$\nu_1^v = -k^2V_v(n^2-\sin^2\theta_o)^{\frac{1}{2}}$$

$$\nu_2^v = 2k_{ox}V_v(n^2-\sin^2\theta_o)^{\frac{1}{2}}\frac{(b+c)}{(c+bn^2)}K_x$$

$$+\frac{kV_v(n^2-1)}{(c+bn^2)}\left[\frac{(n^2-\sin^2\theta_o)}{n^2}(bc+K_y^2)-\sin^2\theta_o(K_x^2+K_y^2)\right] \quad . \qquad (3.14)$$

A problem of considerable interest is that for which only statistical information about the surface is available. We will consider stationary random surfaces, so the average height $\langle\zeta(x)\rangle = 0$, and this implies

$$\langle\bar{A}_1^h\rangle = \langle\bar{A}_1^v\rangle = 0 \quad . \qquad (3.15)$$

The first approximation to the ensemble average of Eq. (2.14) is then

$$\langle e_1^i(-\underset{\sim}{k}_o)\rangle = \left[1-|R_1(\cos\theta_o)|^2\right]-\frac{8\pi^2}{S_o}(\cos\theta_o)\,\mathrm{Re}\left[R_i^*(\cos\theta_o)\langle\beta_2^i(k_{ox},0)\rangle\right]$$

$$-\frac{(2\pi k)^2}{S_o}\int_U d\Omega\,\cos^2\theta\,\langle|\underset{\sim}{A}_1^i(k\sin\theta\cos\phi,k\sin\theta\sin\phi)|^2\rangle \quad , \quad i = h_1v \quad . \qquad (3.16)$$

Thus, the correction to the flat-surface emissivity is second order in surface height.

The expectation values for Eq. (3.16) are easily obtained. Because of the restriction of stationarity, the correlation function of the random process is

$$\left\langle \zeta(x,y)\ \zeta(x+\tau_1,\ y+\tau_2)\right\rangle = \sigma^2 C(\tau) \quad , \tag{3.17}$$

where $\tau = (\tau_1^2+\tau_2^2)$. It can be shown by use of the inverse of Eq. (3.3) that

$$\left\langle S(p_1,q_1)S(p_2,q_2)\right\rangle = W(p_2,q_2)\ \frac{1}{2\pi}\int_o^\infty d\rho\ \rho\ J_o\left[\rho\sqrt{(p_1+p_2)^2+(q_1+q_2)^2}\right] \tag{3.18}$$

Here, the energy spectrum W is the Bessel transform of the correlation function,

$$W(p_1,q_1) = \frac{1}{2\pi}\sigma^2\int_o^\infty d\tau\ \tau\ C(\tau)\ J_o\left[\tau(p_1^2+q_1^2)^{\frac{1}{2}}\right] . \tag{3.19}$$

The other factor in Eq. (3.18) is obviously a delta function but we leave it in integral form because the required expectation values necessitate the choice $p_1 = -p_2$, $q_1 = -q_2$. The infinity arises because of the representation of the incident beam by a plane wave. However, we can relate Eq. (3.18) to the (infinite) beam size S_o defined in Eq. (2.9) by the intermediate step

$$\begin{aligned}\left\langle S(-p,-q)S(p,q)\right\rangle &= W(p,q)\ \frac{1}{2\pi}\lim_{r\to\infty}\int_o^r d\rho\ \rho \\ &= W(p,q)\ \frac{1}{(4\pi\cos\theta_o)}\lim_{r\to\infty} r^2\cos\theta_o \\ &= W(p,q)\ \frac{1}{(2\pi)^2}\ \frac{S_o}{\cos\theta_o} \quad .\end{aligned} \tag{3.20}$$

We can now write down the expectation values required in Eq. (3.16). From Eq. (3.4), we have, say,

$$\left\langle \left|\alpha_1^h\right|^2 \right\rangle = \left|\mu_1^h\right|^2 \left\langle S^*(K_x-k_{ox},K_y)\ S(K_x-k_{ox},K_y)\right\rangle$$

$$= \left|\mu_1^h\right|^2 W(K_x-k_{ox},K_y)\ \frac{S_o}{(2\pi)^2\cos\theta_o} \quad , \tag{3.21}$$

and similarly for the averages of $|\beta_1^h|^2$ and $|\gamma_1^h|^2$. The corresponding result for vertical polarization is

$$\left\langle \left|\alpha_1^v\right|^2 \right\rangle = \left|\mu_1^v\right|^2 W(K_x-k_{ox},K_y)\ \frac{S_o}{(2\pi)^2\cos\theta_o} \quad . \tag{3.22}$$

The second-order averages again follow by use of Eq. (3.20):

$$\left[\cos\theta_o + (n^2-\sin^2\theta_o)^{\frac{1}{2}}\right]\left\langle \beta_2^h(k_{ox},0)\right\rangle$$

$$= \frac{1}{(2\pi)^2}\frac{S_o}{\cos\theta_o}\int_{-\infty}^{\infty}dK_x\int_{-\infty}^{\infty}dK_y\left[\nu_1^h+\nu_2^h(K_x,K_y)\right]W(K_x-k_{ox},K_y) \quad , \tag{3.23}$$

$$\left[n^2\cos\theta_o + (n^2-\sin^2\theta_o)^{\frac{1}{2}}\right]\left\langle \beta_2^v(k_{ox},0)\right\rangle$$

$$= \frac{1}{(2\pi)^2}\left(\frac{S_o}{\cos\theta_o}\right)\int_{-\infty}^{\infty}dK_x\int_{-\infty}^{\infty}dK_y\left[\nu_1^v+\nu_2^v(K_x,K_y)\right]W(K_x-k_{ox},K_y) \quad . \tag{3.24}$$

The area S_o in Eqs. (3.21) - (3.24) cancels the like quantity in Eq. (3.16). Examination of the above results demonstrates that the rough-surface effects on emissivity are determined by the energy spectrum for the surface.

REFERENCES

1. A. Stogryn, "The apparent temperature of the sea at microwave frequencies," IEEE Trans. Ant. and Prop., Vol. AP-15, pp. 278-286, March, 1967.

2. W.H. Peake, "Interaction of electromagnetic waves with some natural surfaces," IRE Trans. Ant. and Prop. (Special Supplement), Vol. AP-7, pp. S324-S329, Dec. 1959.

3. P.J. Lynch and R.J. Wagner, "Rough-surface scattering: shadowing, multiple scatter, and energy conservation," Journ. Math. Phys. Vol. 11, pp. 3032-3042, Oct. 1970.

4. R.J. Wagner and P.J. Lynch, "Theory of high-frequency microwave emission from a rough sea," TRW Systems Technical Report 99994-6100-R0-00, Jan. 1971.

5. P.J. Lynch and R.J. Wagner, "Emission and reflection from anisotropic random rough surfaces," TRW Systems Technical Report No. 17608-6005-R0-00, March, 1972, under ONR Contract N00014-71-C-0240.

6. R.J. Wagner and P.J. Lynch, "Analytical Studies of Scattering and Emission by the Sea Surface," TRW Systems Tech. Report 17608-6006-R0-00, under ONR Contract N00014-71-C-0240, March, 1972.

7. R.J. Wagner and P.J. Lynch, "Sea brightness temperatures at microwave frequencies, "Chap. 31, Propagation Limitations in Remote Sensing, John B. Lomax, ed. Proceedings of the 17th Symposium of the Electromagnetic Wave Propagation Panel of AGARD (NATO/AGARD, Neuilly-sur-Seine, France, 1971).

8. J.P. Hollinger, "Passive microwave measurements of sea surface roughness," IEEE Trans. Geos. Elect., Vol. GE-9, pp. 165-169, July 1971.

9. J.P. Hollinger, "Remote passive microwave measurements of the sea surface," Chapt. 14, Propagation Limitations in Remote Sensing, John B. Lomax, ed. Proceedings of the 17th Symposium of the Electromagnetic Wave Propagation Panel of AGARD (NATO/AGARD, Neuilly-sur-Seine, France; 1971).

10. T.J. Lynch, "Curvature corrections to rough-surface scattering at high frequencies," J. Acoust. Soc. Am. 47, 804 (1970).

11. C. Cox and W. Munk, "Statistics of the sea surface derived from sun glitter," J. Marine Res., Vol. 13, pp. 198-227, 1954.

12. C. Cox and W. Munk, "Measurement of the roughness of the sea surface from photographs of the sun's glitter," Journ. Opt. Soc. of Am., Vol. 44, pp. 838-850, Nov. 1954.

13. Willard J. Pierson, Jr., "A proposed vector wave number spectrum for the study of radar sea return," p. 251, in "Microwave Observations of the Sea Surface" report of a NASA/NAVY Review June 11-12, 1969, prepared by the Spacecraft Oceanography Project of the Naval Oceanographic Office.

14. Jin Wu, "Sea-surface slope and equilibrium wind-wave spectra," Phys. of Fluids, 15, 741-747 (1972).

15. S.O. Rice, "Reflection of electromagnetic waves from slightly rough surfaces," Comm. Pure Appl. Math., Vol. 4, pp. 351-378, 1951.

16. G.R. Valenzuela, "Scattering of electromagnetic waves from a tilted slightly rough surface," Radio Science, Vol. 3 (New Series), pp. 1057-1066, Nov. 1968.

17. D.S. Saxon, "Lectures on the scattering of light," Scientific Report No. 9, Dept. of Meteorology, University of California, Los Angeles, p. 87, May 1955.

18. G.R. Valenzuela, "Depolarization of electromagnetic waves by slightly rough surfaces," IEEE Trans. on Antennas and Propagation, Vol. AP-15, pp. 552-557, July 1967.